

Electronic Supplementary Information

Luminescent ruffled iridium(III) porphyrin complexes containing N-heterocyclic carbene ligands: structures, spectroscopies and potent antitumor activities under dark and light irradiation conditions

Tsz-Lung Lam,^a Ka-Chung Tong,^a Chen Yang,^{ab} Wai-Lun Kwong,^a Xiangguo Guan,^{ab}

Ming-De Li,^a Vanessa Kar-Yan Lo,^a Sharon Lai-Fung Chan,^{lc} David Lee Phillips,^a

*Chun-Nam Lok^{*a} and Chi-Ming Che^{*ab}*

^aState Key Laboratory of Synthetic Chemistry, Institute of Functional Materials, HKU-CAS Joint Laboratory on New Materials and Department of Chemistry, The University of Hong Kong, Pokfulam Road, Hong Kong, China

^bHKU Shenzhen Institute of Research and Innovation, Shenzhen, China

^cDepartment of Applied Biology and Chemical Technology, The Hong Kong Polytechnic University, Hung Hom, Kowloon, Hong Kong, China

E-mail: cnlok@hku.hk

E-mail: cmche@hku.hk

Table of Contents

General considerations	S4
Experimental procedures and characterizations	S11
References	S17
Table S1. Crystallographic data of 2a , 2d , 2e and 2f	S25
Table S2. UV-Visible absorption data of 2e in various organic solvents	S26
Table S3. Natural transition orbitals (NTOs) of the hole and electron pair for S7/S8 and S9/S10 of 2a .	S29
Table S4. The main experimental and calculated Raman bands and their corresponding vibrational mode assignments	S30
Table S5. Mass errors of the fragments detected from Trx peptide (RIMKCPGCWTA) at m/z 422.54 by ESI-MS/MS.	S45
Table S6. Mass errors of the fragments detected from modified Trx peptide (RIMKCPGCWTA) at m/z 421.86 by ESI-MS/MS. Blue label represents the site for disulfide bond formation.	S46
Table S7. Mass errors of the fragments detected from modified Trx peptide (RIMKCPGCWTA) at m/z 427.20 by ESI-MS/MS. Red label indicates the oxidative site and blue label represents the site for disulfide bond formation.	S47
Table S8. Mass errors of the fragments detected from modified Trx peptide (RIMKCPGCWTA) at m/z 433.20 by ESI-MS/MS. Red label indicates the oxidative site.	S48
Fig. S1–S13. ^1H NMR spectra of 1a–2f , 3 , 4 and 1d' .	S18
Fig. S14. UV-vis absorption spectra of $[\text{Ir}^{\text{III}}(\text{F}_{20}\text{tp})\text{Cl}(\text{CO})]$, 1c and 1d in CHCl_3 and 2f in CH_2Cl_2 at 8×10^{-6} M.	S26
Fig. S15. UV-Vis absorption spectra of 2e in various organic solvents at 8×10^{-6} M.	S27
Fig. S16. Emission spectra of 2c–2e in CHCl_3 .	S27
Fig. S17. Emission spectra of 1d , 2f and $[\text{Ir}^{\text{III}}(\text{F}_{20}\text{tp})\text{Cl}(\text{CO})]$ in CHCl_3 .	S28
Fig. S18. DFT optimized structure of 2a .	S28
Fig. S19. $\Delta A_{490\text{nm}}$ decay curves of degassed MeCN solution of 2a (10 μM) and 2a (10 μM) with dibenzylamine (10 mM) as well as $\Delta A_{470\text{nm}}$ decay curves of degassed DMF solution of 2c (10 μM), 2c (10 μM) with 4-chlorophenylboronic acid (2 mM) and 2c (10 μM) with diisopropylamine (8 mM).	S31
Fig. S20. UPLC-QTOF-MS chromatograms of complexes 1d' , 2a , 2c , 2e , 2f , 3 and 4 (1	S32

μM) in DMSO.

Fig. S21 Extracted-ion chromatograms of different complexes and possible DMSO-substituted forms after 5 min and 24 h incubation in DMSO. S34

Fig. S22 Extracted-ion chromatograms of complex **2c** and possible glutathione-substituted forms after 5 min and 24 h incubation in DMSO/ammonium bicarbonate buffer (10 mM) (1:19, v/v). S36

Fig. S23. Plots of cell viability of NCI-H460 lung cancer cells upon 72 h treatment with the iridium(III) porphyrin complexes and *cis*-platin in dark or under light irradiation (2.8 mW cm⁻² for 1 h). S37

Fig. S24. ESI-MS spectra of triply charged peptide (RIMKCPGCWTA, 20 μM) at *m/z* 422.54 after incubation in dark or upon light irradiation for 1 h. S38

Fig. S25. ESI-MS spectra of triply charged peptide (RIMKCPGCWTA, 20 μM) with complex **2c** (10 μM) after incubation in dark or upon light irradiation for 1 h. S39

Fig. S26. MS/MS spectra of triply charged peptide (RIMKCPGCWTA, 20 μM) at *m/z* 422.54 after incubation in dark or upon light irradiation for 1 h. S40

Fig. S27. Flow cytometric analysis of Annexin V/PI double stained NCI-H460 cells treatment with vehicle control, complex **2a**, **2e**, **2f**, **3** and **4** (14 h) in the absence or presence of light irradiation (2.8 mW cm⁻², 1 h). S41

Fig. S28. Cell cycle progression analysis of DAPI-stained NCI-H460 cells treatment with vehicle control, complex **2a**, **2e**, **2f**, **3** and **4** (14 h) in the absence or presence of light irradiation (2.8 mW cm⁻², 1 h) by flow cytometry. S43

Fig. S29. Microscopic examination of the cellular tube formation of MS-1 endothelial cells after treatment with vehicle control, complex **2a**, **2e**, **2f**, **3** and **4** (1 h) in the absence or presence of light irradiation (2.8 mW cm⁻², 1 h). S44

General considerations

Reagents: All reactions were performed in open atmosphere unless otherwise stated. $[\text{Ir}^{\text{III}}(\text{por})\text{Cl}(\text{CO})]$,^{S1,S2} and bis(NHC)silver(I) complexes^{S3} $[\text{Ag}(\text{IMe})_2](\text{OTf})$, $[\text{Ag}(\text{BIMe})_2](\text{OTf})$ and $[\text{Ag}(\text{IPr})_2](\text{PF}_6)$ were prepared according to reported procedures. Other reagents were purchased commercially and used without purification. The solvents used for photophysical measurements were of HPLC grade. The compounds for cell based experiments have sufficient solubility generally up to 20 μM in culture medium after dilution from the DMSO stock; the final concentration of DMSO in the medium was at most 1%.

Instrumentations: ^1H and ^{13}C NMR spectra were recorded on a Bruker AV-400 or DPX-300 spectrometer, chemical shifts were expressed in ppm and were determined with tetramethylsilane (TMS) as internal reference. UV-vis absorption spectra were recorded on a Hewlett-Packard 8452A diode array spectrophotometer or on a Perkin-Lambda 19 UV-vis spectrophotometer. Infra-red (IR) spectra were recorded on a Bio-Rad PTS-165 spectrometer. Positive-ion-mode FAB mass spectra were recorded on a Thermo Scientific DFS high resolution magnetic sector MS. Elemental analyses were performed at the Institute of Chemistry of the Chinese Academy of Sciences, Beijing. Cyclic voltammetry was performed by a Princeton Applied Research Model 73 electrochemical analyzer. A conventional three-compartment electrochemical cell was used. Experiments were conducted with a scan rate of 100 mV/s. A glassy carbon electrode was used as working electrode. A platinum wire and an Ag/AgNO_3 (0.1 M in MeCN) in electrode were used as counter electrode and reference electrode, respectively. $[\text{nBu}_4\text{N}]\text{PF}_6$ solution (0.1 M in CH_2Cl_2) was used as supporting electrolyte. The $E_{1/2}$ of the ferrocenium/ferrocene couple ($\text{Cp}_2\text{Fe}^{+/0}$) measured in the same solution was used as internal standard. TEM samples were prepared by drop casting a few drops of sample dispersion onto a formvar-coated copper grid or onto silicon on the specimen mount, respectively, followed by air-drying in the open atmosphere. TEM images were acquired using a Philips Tecnai GS 20 S-TWIN instrument (accelerating voltage of 200 kV).

Photophysical measurements: Steady state emission spectra at 298 K were obtained on a Spec 1681 Fluorolog-2 Model F111 spectrophotometer equipped with a Hamamatsu R928 PMT detector. All solutions for photophysical measurements, except stated otherwise, were degassed in a high-vacuum line with five freeze-pump-thaw cycles. Emission lifetimes were measured with a Quanta-Ray Q-switch DCR-3 Nd:YAG pulsed laser system. Emission quantum yields of solutions were measured by using a degassed MeCN solution of $[\text{Ru}(\text{bpy})_3](\text{PF}_6)_2$ ($\text{bpy} = 2,2'$ -bipyridine) ($\Phi_{\text{r}} = 0.062$) as the standard and calculated by $\Phi_{\text{s}} = \Phi_{\text{r}}(B_{\text{r}}/B_{\text{s}})(n_{\text{s}}/n_{\text{r}})^2(D_{\text{s}}/D_{\text{r}})$, in which the

subscripts s and r refer to the sample and reference standard solution respectively, n is the refractive index of the solvents, D is the integrated intensity and Φ is the luminescence quantum yield. The quantity B is calculated by $B = 1 - 10^{-AL}$, in which A is the absorbance at the excitation wavelength and L is the optical path length. Errors for wavelength values (1 nm) and Φ (10%) are estimated. Nano-second transient absorption spectra were recorded using a LP920-KS laser flash photolysis spectrometer (Edinburgh Instruments Ltd, Livingston, UK). The excitation source was 355 nm output from a Nd:YAG laser, and the probe light source was a 450 W xenon lamp.

UV-vis spectroelectrochemical measurements: Approximately 1.3 mL of MeCN solution containing $\sim 8 \times 10^{-5}$ M of **2a** and 0.1 M [n Bu₄N]PF₆ was added to a batch-type UV cell designed for spectroelectrochemistry with 1 mm path length. After that, Pt gauze working electrode, Pt counter electrode and pseudo-reference electrode were connected to the same instrument used for cyclic voltammetry. The UV-vis spectra were recorded once constant voltage ($E_{ox} = +0.8$ V; $E_{red} = -1.50$ V vs Ag/AgNO₃ (0.1 M in MeCN)) was applied to the sample solution.

Resonance Raman spectroscopic measurement: Resonance Raman (RR) spectra were measured using 368.9 nm and 435.7 nm excitation wavelength, which are the first and second Anti-Stokes hydrogen Raman-shifted laser line produced from the second harmonic of Nd:YAG laser. The powers of 368.9 nm and 435.7 nm are about 4 mW and 2 mW respectively. The samples were dissolved in acetonitrile solvent with an absorbance of ca. 0.59 at 435.7 nm and ca. 0.29 at 368.9 nm in a 2 mm path-length fused silica cuvette throughout the data acquisition. The excitation laser beam was focused to about a 0.5 mm diameter spot size onto a 2 mm path-length cuvette of sample. A backscattering geometry was employed for sample excitation and for collection of the Raman scattered light by reflective optics. The Raman signal detected by a liquid-nitrogen-cooled charged-coupled device (CCD) detector was acquired for 30 s before being read out to an interfaced personal computer, and 10 of these readouts were averaged to obtain the resonance Raman spectrum. The Raman bands of the MeCN solvent were employed to calibrate the resonance Raman spectra with an estimated accuracy of 5 cm⁻¹ in absolute frequency. The Raman spectrum of the sample was obtained by removing the Raman spectrum of the corresponding solvent with a proper scaling factor.

X-ray crystal structures determinations: X-ray diffraction data of single crystals were collected on Bruker X8 Proteum diffractometer. The crystals were kept at 100 K during data collection. The diffraction images were interpreted and the diffraction intensities were integrated by using the program SAINT. Multi-scan

SADABS was applied for absorption correction. By using OLEX2,^{S4} the structure was solved with the XS^{S5} structure solution program using direct methods and refined with the shelXL^{S6} refinement package using least squares minimization. The positions of the H atoms were calculated on the basis of the riding mode with thermal parameters equal to 1.2 times that of the associated C atoms and these positions participated in the calculation of the final R indices. In the final stage of least-squares refinement, all nonhydrogen atoms were refined anisotropically.

Ultra performance liquid chromatography coupled quadrupole time-of-flight mass spectrometric analysis (UPLC-QTOF-MS): The purity of the iridium(III) porphyrin complexes (**1d'**, **2a**, **2c**, **2e**, **2f**, **3** and **4**) was determined to be > 98%, as examined by UPLC-QTOF mass spectrometry (Fig. S20). For the stability analysis, aliquots from each solution mixture of different iridium(III) complexes in the DMSO solvent (1 μ M) or in the presence of glutathione (2 mM) were obtained at the indicated time and subjected to the UPLC-QTOF-MS analysis. The mobile phase was a mixture of 0.1% formic acid in water (phase A) and 0.1% formic acid in acetonitrile (phase B). Separation was achieved by using 5–100% phase B from 0 to 15 min. The flow rate was 0.4 mL/min and the injection volume was 2 μ L.

Computational details: All calculations were performed using the Gaussian 09 suite of programs.^{S7} The optimized geometry and vibrational frequencies were obtained from B3LYP-GD3BJ/Def2-SVP. The B3LYP-D3 functional incorporating the dispersion proposed by Grimme *et al.* The calculated vibrational frequencies were scaled by a factor of 0.96.

Biological experiments:

Cell culture

HeLa, HepG2, MCF-7 cells were cultured in minimum essential medium (MEM) with fetal bovine serum (10%) and penicillin/streptomycin (100 U/mL, 1%) and maintained at 37 °C in a humidified environment with 5% CO₂. HCT116, HCC827 and NCI-H460 cells were cultured in RPMI-1640 with fetal bovine serum (10%) and penicillin/streptomycin (100 U/mL, 1%) and maintained at 37 °C with 5% CO₂.

Cellular uptake study

NCI-H460 cells were seeded in 12-well plate for 24 h. Then, the cells were treated with different iridium(III) porphyrin complexes (1 μ M) in RPMI culture medium for 2 h. Cells were then washed thrice with PBS. Deionized water (130 μ L) was added onto the cell monolayer for the cell lysis and the cell lysate (100 μ L) were digested in conc. HNO₃ (2:1, v/v) at 70 °C for 18 h. The amount of iridium (μ g/L) in cell lysate was determined by ICP-MS analysis and normalized with the protein content as examined

by Bradford protein assay.

Lipophilicity measurement (Log P)

Iridium(III) porphyrin complexes (40 μM) in 500 μL *n*-octanol (saturated with sodium chloride) was mixed with equal volume of aqueous sodium chloride solution (0.9%, w/v). The mixture was shaken for 24 h at 298 K to allow partitioning. The sample was then centrifuged at 5000 rpm for 10 min to separate two different layers carefully. The samples in each phase were digested in conc. HNO_3 (9:1, v/v) at 70 $^\circ\text{C}$ for 18 h. The amount of iridium ($\mu\text{g/L}$) in two different phases was determined by ICP-MS analysis. The Log *P* was determined as the logarithmic ratio of the concentration of iridium in the *n*-octanol and aqueous phases.

In vitro cytotoxicity (MTT assay)

Different cancer cells were seeded in flat-bottomed 96-well plate, respectively for 24 h in dark. Cells were then incubated with varying concentration of different iridium(III) porphyrin complexes and cisplatin, respectively for 72 h in dark. MTT solution (5 mg/mL, 10 μL) was added into each well for another 4 h of incubation. Cells were then lysed in SDS solution (10%, 100 μL) overnight and the absorbance at 590 nm was read by 96-well plate reader.

Light-induced cytotoxicity assay

NCI-H460 cancer cells were seeded in flat-bottomed 96-well plate for 24 h in dark. Cells were then incubated with varying concentration of different iridium(III) porphyrin complexes and cisplatin, respectively for 24 h in dark. The cells were then exposed to visible light irradiation (2.8 mW cm^{-2}) for 1 h, followed by further incubation in dark for another 24 h. The culture medium was then removed and the remaining cells were fixed with paraformaldehyde (4%) and stained with naphthol blue black solution (0.05%, w/v) overnight. The stained cells were then dissolved in sodium hydroxide (50 mM) and the absorbance at 595 nm was read by 96-well plate reader.

Cell imaging and colocalization studies

NCI-H460 cancer cells were seeded in glass-bottom dishes for 24 h. Then, the cells were treated with complex **2c** (1 μM) in RPMI culture medium for 2 h. The cells were then stained with ER-Tracker green or Mito-Tracker green (50 nM) at 37 $^\circ\text{C}$ for 15 min. The cells were then washed twice with PBS, then imaged with Carl Zeiss LSM 700 confocal laser scanning microscope (CLSM). For complex **2c**: excitation at 555 nm and signal collection from 650 to 750 nm. For ER-Tracker green or Mito-Tracker green: excitation at 488 nm and signal collection at 515 ± 15 nm.

Western blot analysis of ER stress markers

NCI-H460 cancer cells were seeded in 6 cm dishes for 24 h. The cells were treated with complex **2c** (1 μM) in RPMI culture medium for 2, 6 and 24 h. In addition, dose-dependent experiment was performed on the cells at concentrations of 1, 3 and 5 μM , respectively, for 6 h. The cells were then harvested and lysed with lysis buffer (1%

Triton X-100, 100 mM Tris-HCl pH 7.4, 140 mM NaCl, 2 mM EDTA, 0.1% SDS, 10% glycerol, 10 mM NaF, 5 mM sodium orthovanadate) with protease inhibitor cocktail. The cell lysate was subjected to centrifugation at 14000 rpm, 4 °C for 15 min. The total protein content in liquid supernatant of each sample was quantified by Bradford's assay. 25 µg of proteins was reconstituted in loading buffer (50 mM DTT, 1X protein loading dye) and heated at 95 °C for 5 min. The protein mixtures were resolved on 10% SDS-PAGE gel by electrophoresis and blotted on polyvinylidene fluoride (PVDF) membranes. The membrane was then blocked with 3% BSA in TBST buffer and incubated with corresponding primary antibodies at 4 °C overnight and the appropriate secondary antibodies for further 2 h. The protein bands were visualized by the chemiluminescence kit (ECL, Amersham). Equal loading of each lane was confirmed by the intensity of β -actin. The following antibodies were used: Phospho-eIF2 α (Ser51), CHOP (D46F1) and β -actin (13E5) from Cell Signaling Technology.

Mitochondrial depolarization assay

NCI-H460 cancer cells were seeded in flat-bottomed and black 96-well plate for 24 h. The cells were treated with complex **2c** (1 µM) and DMSO vehicle in RPMI culture medium for 2 and 6 h. JC-1 (5 µM) staining solution was then added to the cells and incubation was continued for 20 min in dark. After washing the cells with serum free culture medium and PBS for twice, the fluorescence intensities for both J-aggregates and monomeric forms of JC-1 were measured with a 96-well plate reader (J-aggregates: excitation/emission = 488/585 nm; JC-1 monomers: excitation/emission = 488/530 nm). For positive control, carbonylcyanide *m*-chlorophenylhydrazone (CCCP, 50 µM) and JC-1 (5 µM) were co-incubated with the cells for 15 min and the fluorescence intensity was measured under the same conditions.

Intracellular detection and measurement of ROS generation

The intracellular ROS generation triggered by complex **2c** in NCI-H460 cancer cells in dark or upon visible light irradiation was measured using DCF-DA as the ROS probe. After the treatment of NCI-H460 cells with **2c** at 37 °C for 2 h in dark, cells were further incubated with DCF-DA (10 µM) for 15 min. Subsequently, cells were washed twice with PBS and replaced with fresh medium and further exposed to visible light irradiation (2.8 mW cm⁻²) for 1 h. Cells were lysed by Triton X-100 (0.1%, v/v) and the fluorescent intensity of the cell lysate was measured with excitation at 488 nm and emission at 520 ± 10 nm. For visualization of the intracellular ROS generation, the cells treated in dark or upon light irradiation were imaged with CLSM.

Identification of the oxidative modification on peptide by mass spectrometry

The peptide (RIMKCPGCWTA, 20 µM) was freshly prepared together with complex **2c** in 10 mM ammonium bicarbonate buffer (with 10% MeCN, v/v). The reaction mixture was subjected to incubate in dark or upon visible light irradiation (2.8 mW cm⁻²) for 1 h and the samples were then diluted with 50% MeCN with 0.1% formic acid

and subjected to high resolution ESI-QTOF-MS analysis (Brucker maXis II). The peptide alone was also prepared as a control.

Apoptosis and necrosis assays

Induction of apoptosis or necrosis in cells was determined by the Annexin V-FITC/Propidium iodide staining assay using flow cytometry. Briefly, NCI-H460 cancer cells were treated with different iridium(III) porphyrin complexes for 3 h in dark. The cells were then exposed to visible light irradiation (2.8 mW cm^{-2}) for 1 h, followed by further incubation in dark for another 14 h. Cells were harvested by trypsinization, centrifugation and resuspended in binding buffer (10 mM Hepes, 140 mM NaCl, and 2.5 mM CaCl_2 , pH 7.4), followed by staining with Annexin V-FITC and propidium iodide (PI, 50 $\mu\text{g/mL}$) for 20 min at room temperature. Samples were then subjected to flow cytometry analysis with FITC (excitation at 488 nm, emission from 515-545 nm) and PE Texas Red channels (PI, excitation at 561 nm, emission from 580-595 nm). Data were analyzed by FlowJo software.

Cell cycle analysis

NCI-H460 cancer cells were treated with different iridium(III) porphyrin complexes for 3 h in dark. The cells were then exposed to visible light irradiation (2.8 mW cm^{-2}) for 1 h, followed by further incubation in dark for another 14 h. Cells were then washed with PBS twice and detached using Trypsin. After centrifugation (1000 rpm, 5 min), cells were fixed in cold ethanol (70%) for 30 min, centrifuged and resuspended in PBS. DAPI solution was added into the sample solutions to give final concentration of 1 $\mu\text{g/mL}$. The samples were subjected to flow cytometry analysis with Pacific blue channels (excitation at 405 nm, emission from 430-470 nm).

Tube formation assay

MS-1 mouse pancreatic islet endothelial cells on the flat-bottomed 96-well plate with each well coated with basement membrane matrix (Matrigel) were treated with different iridium(III) porphyrin complexes for 1 h in dark. The cells were then exposed to visible light irradiation (2.8 mW cm^{-2}) for 1 h, followed by further incubation in dark for another 2 h. The images of the endothelial cell tube formation were captured under light microscope.

In vivo antitumor study

All animal experiments were conducted under the guidelines approved by the Committee on the Use of Live Animals in Teaching and Research of the University of Hong Kong. Balb/cAnN-nu nude mice (~6–7 weeks old) were obtained from Charles River Laboratory (Wilmington, MA). To generate the NCI-H460 tumors, 4×10^6 NCI-H460 cells suspended in PBS (100 μL) were subcutaneously injected into the right back flank of each mouse. The mice were started to treat when the tumor volumes reached about 50 mm^3 ; the mice were randomly divided into two groups with five mice per group for (A) vehicle control and (B) complex **2c** (3 mg/kg). Mice were treated with

vehicle control or **2c** according to the body weight thrice weekly by intravenous injection until the mice were sacrificed after 16 days of treatment. Tumor sizes were measured thrice weekly and the tumor volumes were calculated by the formula ($V = ab^2 \times 0.52$; where a and b represent the length and width of the tumor). Vehicle control was 1.5% PET in PBS (v/v) (PET: 60% poly(ethylene glycol); 30% ethanol; 10% tween 80).

In vivo photodynamic therapy study

Twenty Balb/cAnN-nu nude mice (~6–7 weeks old) inoculated with NCI-H460 lung tumor xenografts were divided into four groups including vehicle control (PET 1.5%), complex **2c** (3 mg/kg), vehicle control with light irradiation and **2c** (3 mg/kg) with light irradiation. When the tumor reached 50–100 mm³, Mice were treated with vehicle control or **2c** according to the body weight on the first and seventh days by intratumoral injection (50 µL). At 15 min post-injection, for the PDT group, the tumor-bearing mice were anesthetized with xylazine (7.5 mg/kg) and the tumor site was exposed to irradiate at 110 mW cm⁻² for 30 min. Another two groups without light irradiation served as dark control. Tumor sizes were measured thrice weekly and the tumor volumes were calculated by the formula ($V = ab^2 \times 0.52$; where a and b represent the length and width of the tumor).

Experimental procedures and characterizations

Synthesis of [Ir^{III}(por)Cl(CO)]: A mixture of free porphyrin ligand (0.5 mmol) and [Ir(COD)Cl₂]₂ (2 equiv.) in 1,2,4-trichlorobenzene (20 mL) was heated to 185 °C in open atmosphere for 1.5 to 36 h. The progress of reaction was monitored by TLC (until the disappearance of spot of free porphyrin ligand). The reaction mixture was allowed to cool down to room temperature. The crude mixture was purified by silica gel column chromatography using hexane (toluene for [Ir^{III}(oep)Cl(CO)]), then hexane/CH₂Cl₂ as eluent.

[Ir^{III}(ttp)Cl(CO)]:^{S8} Yield: 53%. ¹H NMR (400 MHz, CDCl₃): δ 8.96 (s, 8H), 8.16 (d, 4H, *J* = 6.9Hz), 8.10 (d, 4H, *J* = 6.9Hz), 7.58 (d, 8H, *J* = 8.2Hz), 2.72 (s, 12H). IR (KBr disc, cm⁻¹): ν = 2044 (CO), 1017 (“oxidation state marker band”).

[Ir^{III}(oep)Cl(CO)]:^{S9} Yield: 45%. ¹H NMR (400 MHz, CDCl₃): δ 10.31 (s, 4H), 4.20–4.09 (m, 16H), 2.02 (t, 24H, *J* = 7.7Hz). IR (KBr disc, cm⁻¹): ν = 2041(CO), 1022 (“oxidation state marker band”).

[Ir^{III}(tmp)Cl(CO)]:^{S10} Yield: 62%. ¹H NMR (400 MHz, CDCl₃): δ 8.66 (s, 8H), 7.28 (s, 8H), 2.62 (s, 12H), 1.92 (s, 12H), 1.83 (s, 12H). IR (KBr disc, cm⁻¹): ν = 2047 (CO), 1022 (“oxidation state marker band”).

[Ir^{III}(F₂₀ttp)Cl(CO)]:^{S2, S11} Yield: 38%. ¹H NMR (400 MHz, CDCl₃): δ 9.01 (s, 8H). ¹⁹F NMR (376 MHz, CDCl₃): -134.7 (dd), -136.8 (dd), -150.2 (t), -160.4 (td), -161.0 (td); IR (KBr disc, cm⁻¹): ν = 2063(CO), 1026 (“oxidation state marker band”).

Synthesis of mono(NHC)iridium(III) porphyrin complexes [Ir^{III}(por)(NHC)Cl] 1 (por = tmp or F₂₀ttp; NHC = IMe or BIme): To a CH₂Cl₂ solution (15 mL) of [Ir^{III}(por)Cl(CO)] (0.08 mmol, 1 equiv.), [Ag(NHC)₂](OTf) (0.5 equiv.) was added. The mixture was stirred at room temperature for 12 h. After the complete consumption of [Ir^{III}(por)Cl(CO)] as indicated by TLC analysis of the crude reaction mixture, AgCl salt was removed by filtering through a short pad of either Celite (using CH₂Cl₂/hexane (1:1 v/v) as the eluent (when por = tmp)) or silica gel (using CH₂Cl₂/EtOAc (95:5 v/v) as the eluent (when por = F₂₀ttp)). The desired complex was further purified by recrystallization in a solution of CH₂Cl₂/hexane.

[Ir^{III}(tmp)(IMe)Cl] **1a**: Yield: 74%. ¹H NMR (400 MHz, CDCl₃) δ 8.32 (s, 8H), 7.14 (s, 8H), 4.72 (s, 2H), 2.52 (s, 12H), 1.76 (s, 12H), 1.70 (s, 12H), -0.17 (s, 6H). IR (KBr disc, cm⁻¹): ν = 1018 (“oxidation state marker band”). FAB-MS (*m/z*): 1068 [M – Cl]⁺. Elemental analysis calcd. (%) for C₆₁H₆₀ClIrN₆: C 66.31, H 5.47, N 7.61; Found C

66.42, H 5.30, N 7.67.

[Ir^{III}(tmp)(BIme)Cl] **1b**: Yield: 65%. ¹H NMR (400 MHz, CDCl₃) δ 8.36 (s, 8H), 7.14 (s, 4H), 7.09 (s, 4H), 6.52–6.49 (m, 2H), 6.00–5.98 (m, 2H), 2.51 (s, 12H), 1.70 (s, 12H), 1.63 (s, 12H), -0.01 (s, 6H). IR (KBr disc, cm⁻¹): ν = 1019 (“oxidation state marker band”). FAB-MS (*m/z*): 1120 [M – Cl]⁺. Elemental analysis calcd. (%) for C₆₅H₆₂ClIrN₆: C 67.60, H 5.41, N 7.28; Found C 67.32, H 5.57, N 7.29.

[Ir^{III}(F₂₀tpp)(Ime)Cl] **1c**: Yield: 60%. ¹H NMR (300 MHz, CDCl₃) δ 8.58 (s, 8H), 4.71 (s, 2H), -0.27 (s, 6H). ¹⁹F NMR (376 MHz, CDCl₃) δ -136.2 (dd), -138.7 (dd), -152.8 (t), -161.8 (td), -163.0 (td). IR (KBr disc, cm⁻¹): ν = 1021 (“oxidation state marker band”). FAB-MS (*m/z*): 1260 [M – Cl]⁺.

[Ir^{III}(F₂₀tpp)(BIme)Cl] **1d**: Yield: 61%. ¹H NMR (400 MHz, CDCl₃) δ 8.62 (s, 8H), 6.55–6.53 (m, 2H), 6.01–5.98 (m, 2H), -0.12 (s, 6H). ¹⁹F NMR (376 MHz, CDCl₃) δ -134.0 (dd), -138.3 (dd), -151.5 (t), -160.5 (td), -162.1 (td). IR (KBr disc, cm⁻¹): ν = 1021 (“oxidation state marker band”). FAB-MS (*m/z*): 1311 [M – Cl]⁺. Elemental analysis calcd. (%) for C₅₃H₁₈ClF₂₀IrN₆: C 47.28, H 1.35, N 6.24; Found C 47.18, H 1.42, N 6.15.

Synthesis of cationic bis(NHC)iridium(III) porphyrin complexes [Ir^{III}(por)(NHC)₂]⁺ **2 (por = ttp, oep or F₂₀tpp; NHC = Ime, IⁱPr or BIme):** To a CH₂Cl₂ solution (10 mL) of [Ir^{III}(por)Cl(CO)] (0.08 mmol, 1 equiv.), [Ag(NHC)₂]⁺ (1.05 equiv.) was added. The mixture was stirred at room temperature (under reflux condition for complex **2f**, where por = F₂₀tpp, NHC = Ime). After complete consumption of [Ir^{III}(por)Cl(CO)] as indicated by TLC analysis of the crude reaction mixture, the reaction mixture was concentrated under reduced pressure. The desired complex was purified by flash column chromatography on silica gel using CH₂Cl₂/EtOAc (1:1 – 1:4 v/v) as eluent.

[Ir^{III}(ttp)(Ime)₂](OTf) **2a**: Reaction time: 18 h. Yield: 96%. ¹H NMR (400 MHz, CDCl₃) δ 8.61 (s, 8H), 7.64 (d, *J* = 7.6 Hz, 8H), 7.46 (d, *J* = 7.8 Hz, 8H), 4.83 (s, 4H), 2.63 (s, 12H), -0.57 (s, 12H). ¹⁹F NMR (376 MHz, CDCl₃) δ -78.5 (OTf). IR (KBr disc, cm⁻¹): ν = 1031 (OTf), 1018 (“oxidation state marker band”). FAB-MS (*m/z*): 1053 [M]⁺. Elemental analysis calcd. (%) for C₅₉H₅₂F₃IrN₈O₃S: C 58.94, H 4.36, N 9.32; Found C 59.02, H 4.47, N 9.01.

[Ir^{III}(ttp)(Ime)₂](PF₆) **2a·PF₆** was prepared by anion exchange of **2a** with excess NH₄PF₆ in MeOH. Diffraction-quality crystal was obtained by layering hexane onto concentrated CH₂Cl₂/Et₂O solution.

[Ir^{III}(ttp)(BIme)₂](OTf) **2b**: Reaction time: 18 h. Yield: 90%. ¹H NMR (400 MHz, CDCl₃) δ 8.69 (s, 8H), 7.54 (d, *J* = 7.9 Hz, 8H), 7.42 (d, *J* = 7.9 Hz, 8H), 6.64–6.62 (m, 4H), 6.10–6.07 (m, 4H), 2.60 (s, 12H), -0.41 (s, 12H). ¹⁹F NMR (376 MHz, CDCl₃) δ -78.5 (OTf⁻). IR (KBr disc, cm⁻¹): ν = 1030 (OTf⁻), 1018 (“oxidation state marker band”). FAB-MS (*m/z*): 1153 [M]⁺. Elemental analysis calcd. (%) for C₆₇H₅₆F₃IrN₈O₃S: C 61.78, H 4.33, N 8.60; Found C 61.97, H 4.40, N 8.42.

[Ir^{III}(oep)(Ime)₂](OTf) **2c**: Reaction time: 12 h. Yield: 88%. ¹H NMR (400 MHz, CDCl₃) δ 9.39 (s, 4H), 4.53 (s, 4H), 3.89 (q, *J* = 7.6 Hz, 16H), 1.82 (t, *J* = 7.6 Hz, 24H), -0.96 (s, 12H). ¹⁹F NMR (376 MHz, CDCl₃) δ -78.5 (OTf⁻). IR (KBr disc, cm⁻¹): ν = 1031 (OTf⁻), 1022 (“oxidation state marker band”). FAB-MS (*m/z*): 917 [M]⁺. Elemental analysis calcd. (%) for C₄₇H₆₀F₃IrN₈O₃S: C 52.94, H 5.67, N 10.51; Found C 52.54, H 5.63, N 10.31.

[Ir^{III}(oep)(BIme)₂](OTf) **2d**: Reaction time: 12 h. Yield: 87%. ¹H NMR (400 MHz, CDCl₃) δ 9.45 (s, 4H), 6.49–6.48 (m, 4H), 5.92–5.88 (m, 4H), 3.91 (q, *J* = 7.6 Hz, 16H), 1.83 (t, *J* = 7.6 Hz, 24H), -0.82 (s, 12H). ¹⁹F NMR (376 MHz, CDCl₃) δ -78.5 (OTf⁻). IR (KBr disc, cm⁻¹): ν = 1031 (OTf⁻), 1020 (“oxidation state marker band”). FAB-MS (*m/z*): 1017 [M]⁺. Elemental analysis calcd. (%) for C₅₅H₆₄F₃IrN₈O₃S: C 56.63, H 5.53, N 9.61; Found C 56.92, H 5.43, N 9.65.

[Ir^{III}(oep)(BIme)₂](PF₆) **2d**·PF₆ was prepared by anion exchange of **2d** with excess NH₄PF₆ in MeOH. Diffraction-quality crystal was obtained by layering hexane onto concentrated CH₂Cl₂/Et₂O solution.

[Ir^{III}(oep)(IⁱPr)₂](PF₆) **2e**: Reaction time: 14 h. Yield: 85%. ¹H NMR (400 MHz, CDCl₃) δ 9.40 (s, 4H), 4.84 (s, 4H), 3.95–3.80 (m, 16H), 1.88 (t, *J* = 7.6 Hz, 24H), -0.67 (d, *J* = 6.7 Hz, 24H), -3.14 (sep, *J* = 6.7 Hz, 4H). ¹⁹F NMR (376 MHz, CDCl₃) δ -73.2, -75.1 (PF₆⁻). IR (KBr disc, cm⁻¹): ν = 1022 (“oxidation state marker band”), 839 (PF₆⁻). FAB-MS (*m/z*): 1029 [M]⁺. Elemental analysis calcd. (%) for C₅₄H₇₆F₆IrN₈P: C 55.23, H 6.52, N 9.54; Found C 55.01, H 6.55, N 9.28. Diffraction-quality crystal was obtained by layering hexane onto concentrated CH₂Cl₂ solution.

[Ir^{III}(F₂₀tp)₂](Ime)₂](OTf) **2f**: Reaction time: 4 d (additional 1.2 equiv. of bis(NHC)Ag complex was added on the 3rd day). Yield: 70%. ¹H NMR (400 MHz, CD₂Cl₂) δ 8.70 (s, 8H), 4.76 (s, 4H), -0.55 (s, 12H). ¹³C NMR (125 MHz, CD₂Cl₂) δ 133.7 (Ir–C_{NHC}). ¹⁹F NMR (376 MHz, CD₂Cl₂) δ -78.5 (OTf⁻), -138.3 (dd), -149.6 (t), -160.0 (td). IR (KBr disc, cm⁻¹): ν = 1031 (OTf⁻), 1019 (“oxidation state marker band”). FAB-MS (*m/z*): 1356 [M]⁺. Elemental analysis calcd. (%) for C₅₅H₂₄F₂₃IrN₈O₃S: C 43.86, H 1.61, N

7.44; Found C 43.69, H 1.62, N 7.38. Diffraction-quality crystal was obtained by layering hexane onto concentrated CH₂Cl₂/Et₂O solution.

Synthesis of [Ir^{III}(oep)(CNPhOMe)₂](BF₄) (3): To a 10 mL anhydrous CH₂Cl₂ solution of [Ir(oep)Cl(CO)] (0.05 mmol) and 3 equiv. of AgBF₄, 5 equiv. of 4-methoxyphenyl isocyanide was added under N₂ atmosphere. The reaction mixture was refluxed for 24 h in the absence of light. The solvent was removed under reduced pressure. The residue was purified by column chromatography on alumina using CH₂Cl₂/MeCN (9:1 v/v) as eluent.

Yield: 58%. ¹H NMR (400 MHz, CDCl₃) δ 10.31 (s, 4H), 5.99 (d, *J* = 8.0 Hz, 4H), 4.75 (d, *J* = 8.0 Hz, 4H), 4.20 (q, *J* = 7.6 Hz, 16H), 3.36 (s, 6H), 2.01 (t, *J* = 7.6 Hz, 24H). FAB-MS (*m/z*): 991 [M]⁺. Elemental analysis calcd. (%) for C₅₂H₅₈BF₄IrN₆O₂: C 57.93, H 5.42, N 7.80; Found C 57.52, H 5.62, N 7.78.

Synthesis of [Ir^{III}(oep)(py)₂](Cl) (4): The synthesis follows the literature method.^{S1} Yield: 42%. ¹H NMR (400 MHz, CDCl₃): δ 10.22 (s, 4H), 6.07 (t, *J* = 7.6 Hz, 2H), 4.94 (t, *J* = 7.1 Hz, 4H), 4.12 (q, *J* = 7.6 Hz, 16H), 1.92 (t, *J* = 7.6 Hz, 24H), 0.25 (d, *J* = 5.8 Hz, 4H).

Synthesis of [Ir^{III}(F₂₀tpp)(BIMe)(NH₃)](PF₆) (1d'): To a 10 mL CH₂Cl₂ solution of **1d** (0.02 mmol) was treated with 30 equiv. NH₄PF₆. The suspension was stirred at room temperature for 36 h. The mixture was filtered through a plug of celite followed by recrystallization from a solution of CH₂Cl₂/hexane.

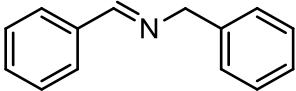
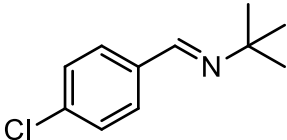
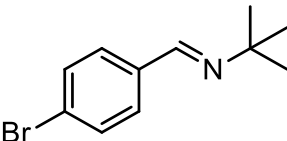
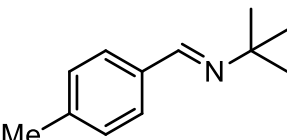
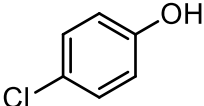
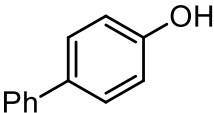
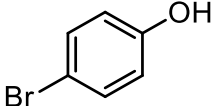
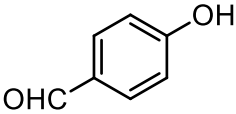
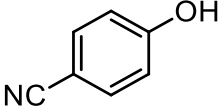
Yield: 90%. ¹H NMR (400 MHz, CDCl₃) δ 8.82 (s, 8H), 6.59–6.57 (m, 2H), 6.03–6.00 (m, 2H), -0.22 (s, 6H), -5.13 (s, 3H). ¹⁹F NMR (376 MHz, CDCl₃) δ -73.9, -75.8 (PF₆⁻), -134.8 (d), -138.6 (d), -149.8 (t), -159.1(td), -161.1(td). FAB-MS (*m/z*): 1328 [M]⁺. Elemental analysis calcd. (%) for C₅₃H₂₁F₂₆IrN₇P: C 43.22, H 1.44, N 6.66; Found C 43.69, H 1.48, N 6.58.

General procedure of light-induced oxidation of secondary amines: A mixture of secondary amine (0.1 mmol) and **2a/2c** (0.1 μmol) in 1.5 mL MeCN was irradiated with Xenon lamp equipped with a 399 nm-filter under a slow stream of O₂ bubbling for 5 h at room temperature. Solvent was removed under reduced pressure to afford the crude mixture. NMR yield was determined by ¹H NMR analysis of the crude reaction mixture using 1,1-diphenylethylene as the internal standard.

General procedure of light-induced oxidation of arylboronic acids: A mixture of arylboronic acid (0.1 mmol), diisopropylamine (0.4 mmol) and **2c** (0.5 μmol) in 1.5 mL DMF with a slow stream of O₂ bubbling was irradiated with Xenon lamp equipped

with a 399 nm-filter under a slow stream of O₂ bubbling for 3 h at room temperature. The reaction was quenched by addition of 1 mL HCl (1 M). The mixture was extracted with diethyl ether. The organic layer was dried with Mg₂SO₄ and solvent was removed under reduced pressure to afford the crude mixture. NMR yield was determined by ¹H NMR analysis of the crude reaction mixture using 1,1-diphenylethylene as the internal standard.

Literature references of light-induced oxidation reaction products:

Product	References
	C. A. Newman, J. C. Antilla, P. Chen, A. V. Predeus, L. Fielding and W. D. Wulff, <i>J. Am. Chem. Soc.</i> , 2007, 129 , 7216-7217.
	S. Tussing, K. Kaupmees and J. Paradies, <i>Chem. Eur. J.</i> , 2016, 22 , 7422-7426.
	
	
	
	R. B. Wagh and J. M. Nagarkar, <i>Tetrahedron Lett.</i> , 2017, 58 , 4572-4575.
	
	C. Zhu, R. Wang and Falck, <i>Org. Lett.</i> , 2012, 14 , 3494-3497.
	

References

- S1 K. Koren, S. M. Borisov, R. Saf and I. Klimant, *Eur. J. Inorg. Chem.*, 2011, 1531-1534.
- S2 J.-C. Wang, Y. Zhang, Z.-J. Xu, V. K.-Y. Lo and C.-M. Che, *ACS Catal.*, 2013, **3**, 1144-1148.
- S3 U. Hintermair, U. Englert and W. Leitner, *Organometallics*, 2011, **30**, 3726-3731.
- S4 O. V. Dolomanov, L. J. Bourhis, R. J. Gildea, J. A. K. Howard and H. Puschmann, *J. Appl. Crystallogr.*, 2009, **42**, 339-341.
- S5 G. M. Sheldrick, *Acta Crystallogr.*, 2008, **A64**, 112-122.
- S6 G. M. Sheldrick, *Acta Crystallogr.*, 2015, **C71**, 3-8.
- S7 G. A. Crosby and J. N. Demas, *J. Phys. Chem.*, 1971, **75**, 991-1024.
- S8 S. K. Yeung and K. S. Chan, *Organometallics*, 2005, **24**, 6426-6430.
- S9 H. Ogoshi, J.-I. Setsune and Z.-I. Yoshida, *J. Organomet. Chem.*, 1978, **159**, 317-328.
- S10 J. P. Collman, L. L. Chng and D. A. Tyvoll, *Inorg. Chem.*, 1995, **34**, 1311-1324.
- S11 A. Delgado-Lima, A. M. Fonseca and A. V. Machado, *Mater. Lett.*, 2017, **200**, 6-9.

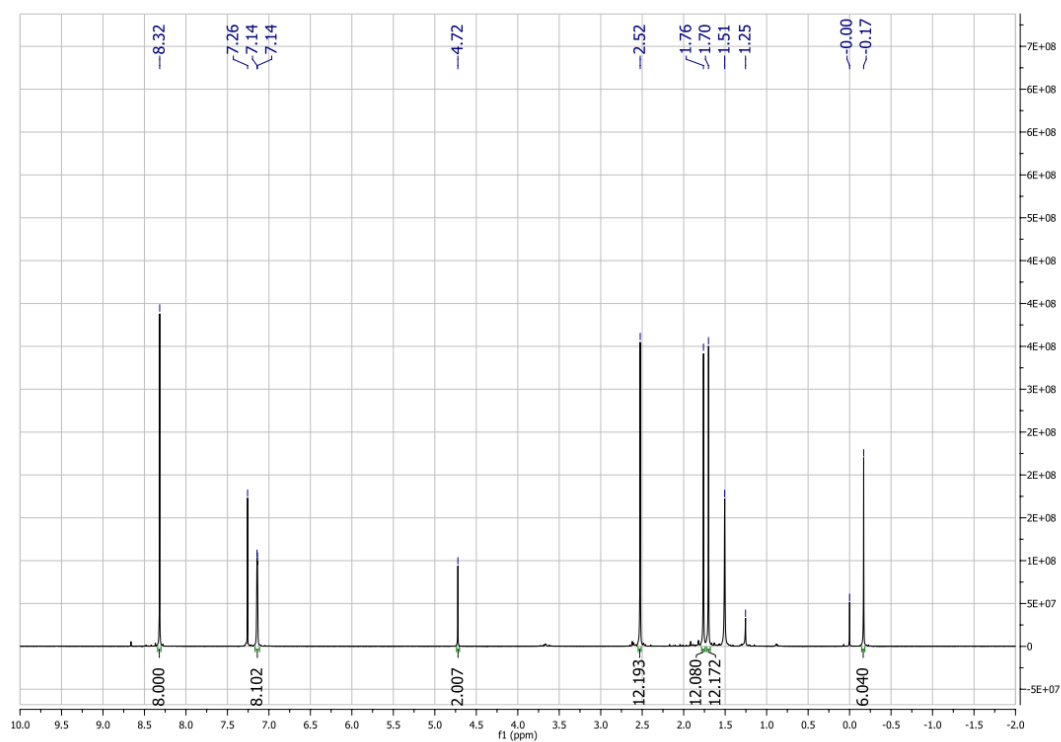


Fig. S1 ^1H NMR (400 MHz, CDCl_3) spectrum of **1a**.

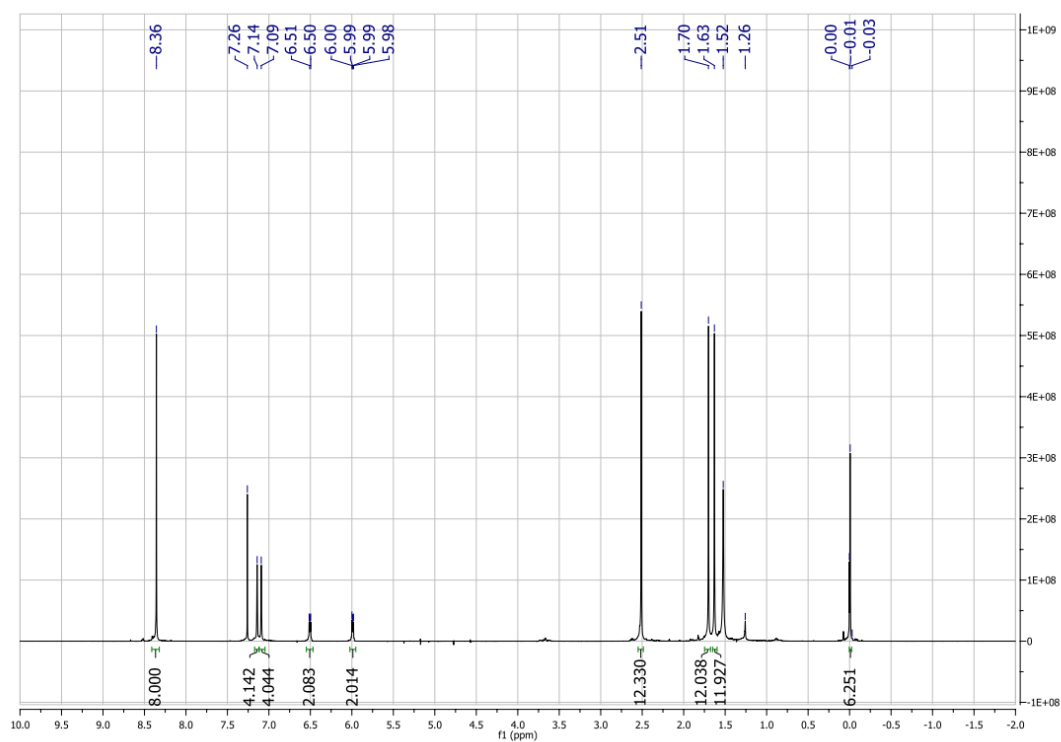


Fig. S2 ^1H NMR (400 MHz, CDCl_3) spectrum of **1b**.

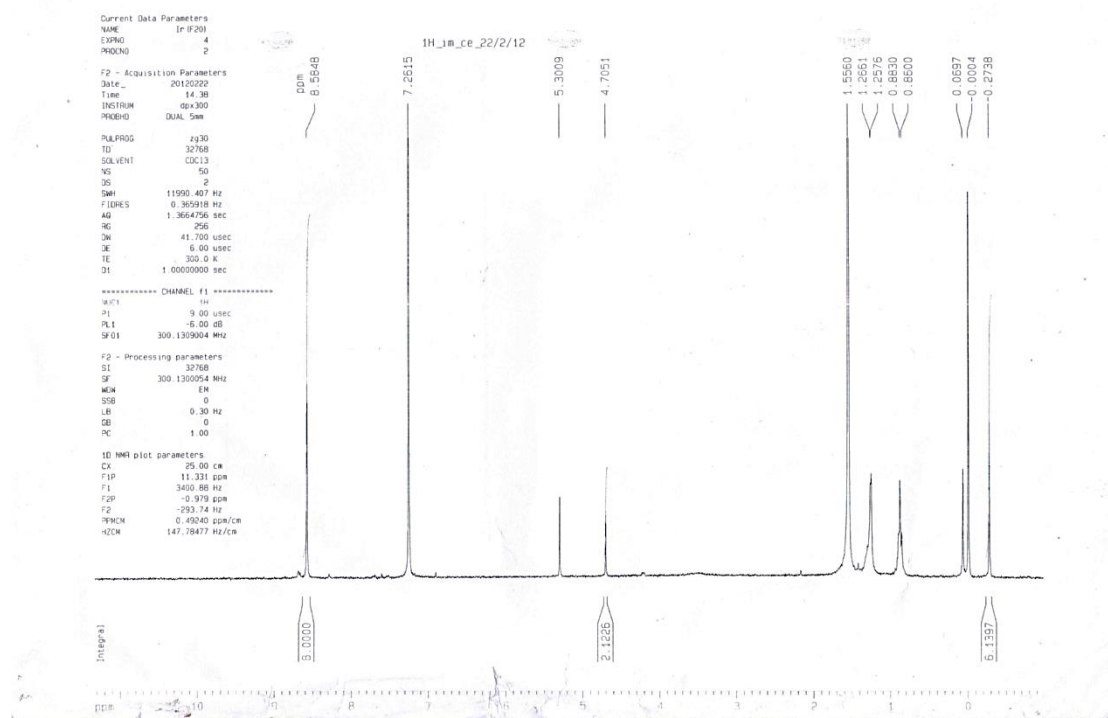


Fig. S3 ^1H NMR (300 MHz, CDCl_3) spectrum of **1c**.

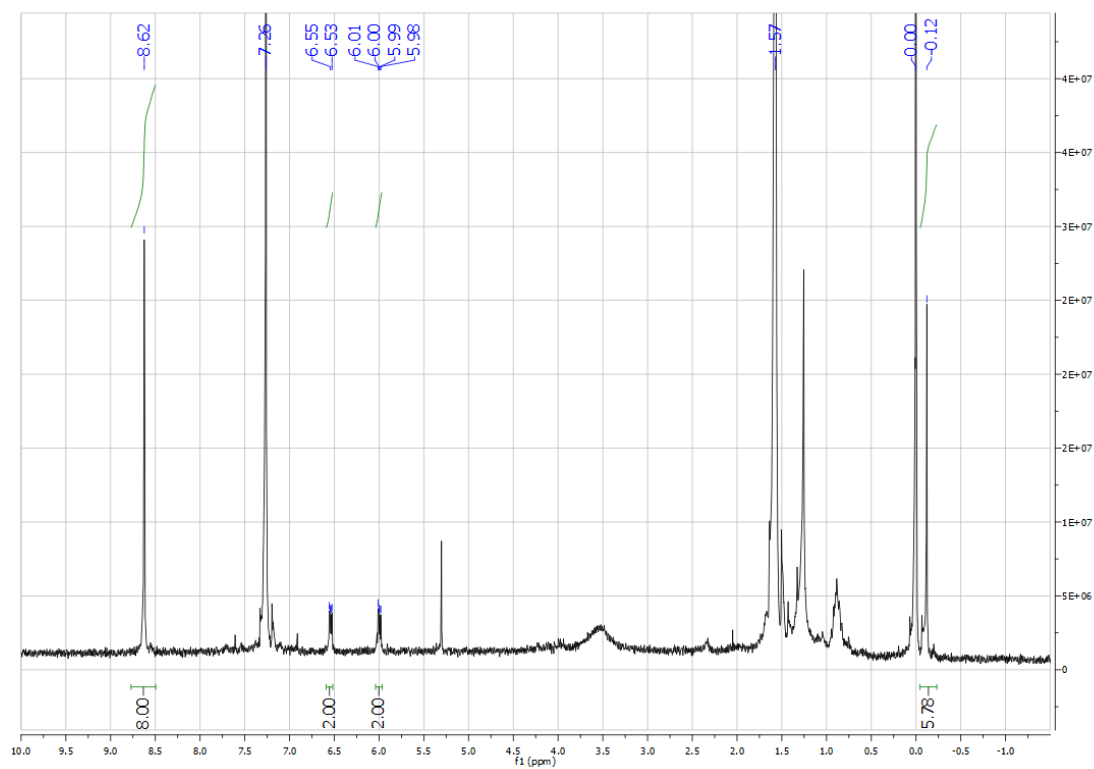


Fig. S4 ^1H NMR (400 MHz, CDCl_3) spectrum of **1d**.

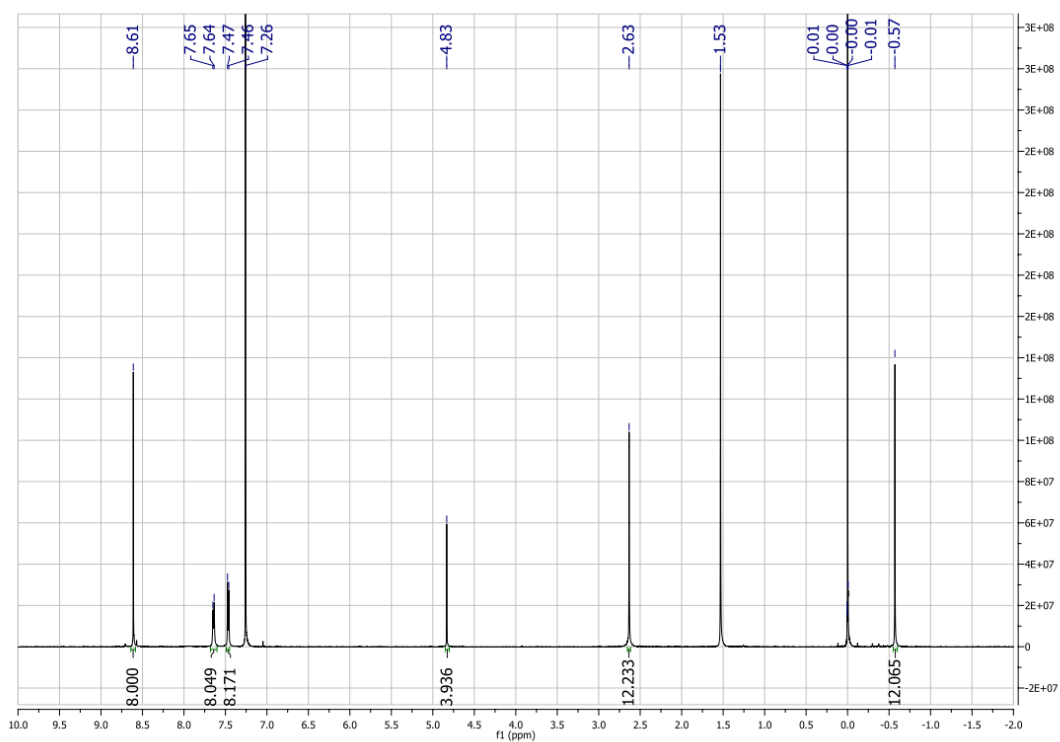


Fig. S5 ¹H NMR (400MHz, CDCl₃) spectrum of **2a**.

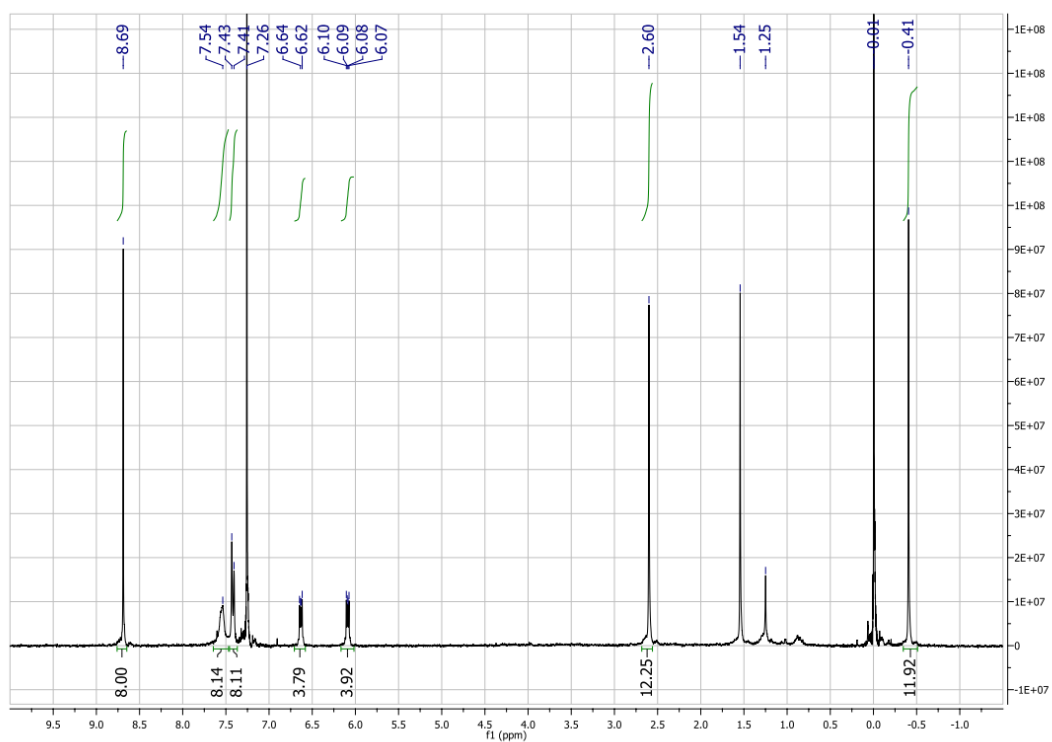


Fig. S6 ¹H NMR (400 MHz, CDCl₃) spectrum of **2b**.

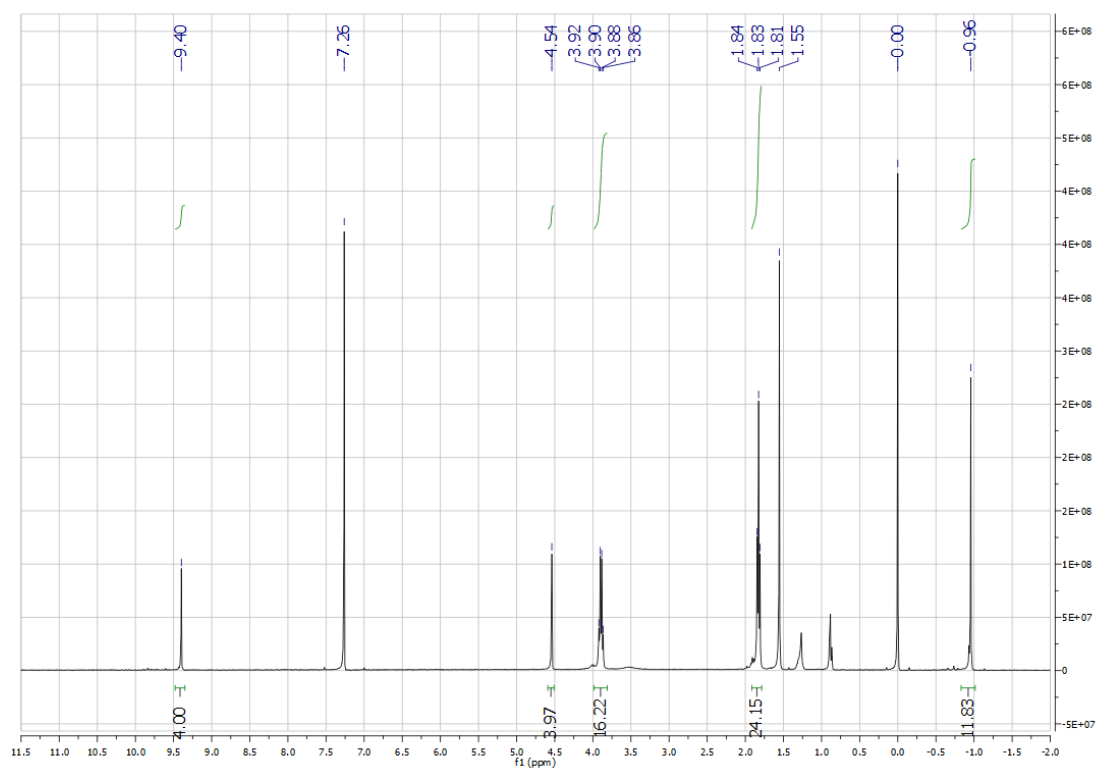


Fig. S7 ^1H NMR (400 MHz, CDCl_3) spectrum of **2c**.

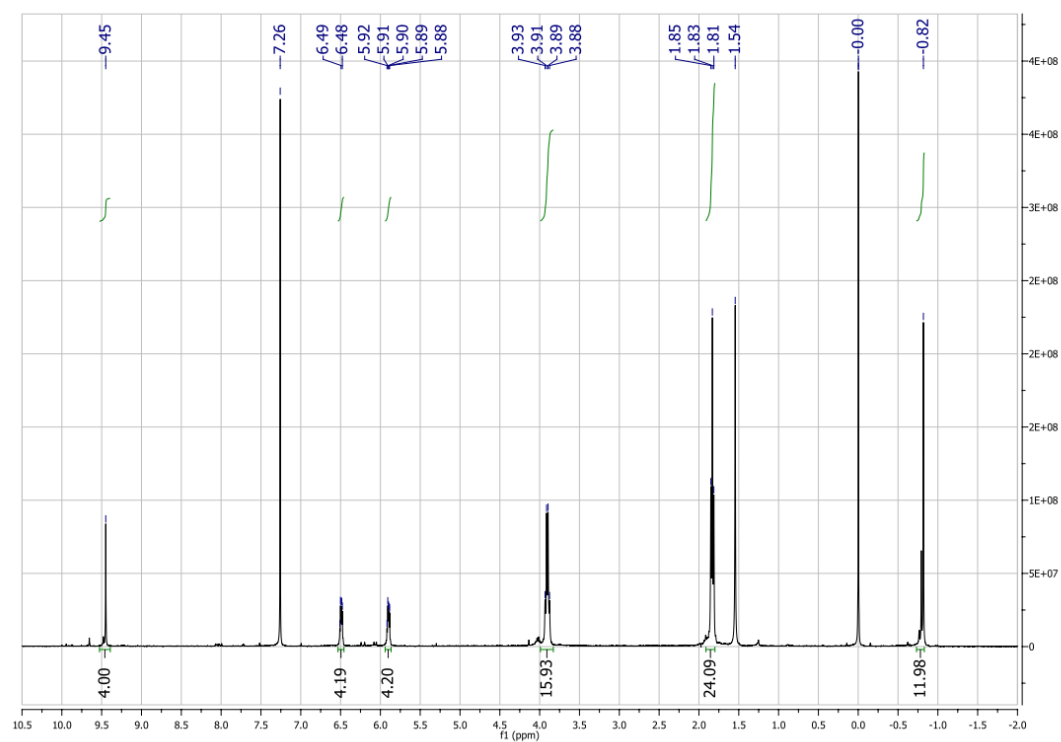


Fig. S8 ^1H NMR (400 MHz, CDCl_3) spectrum of **2d**.

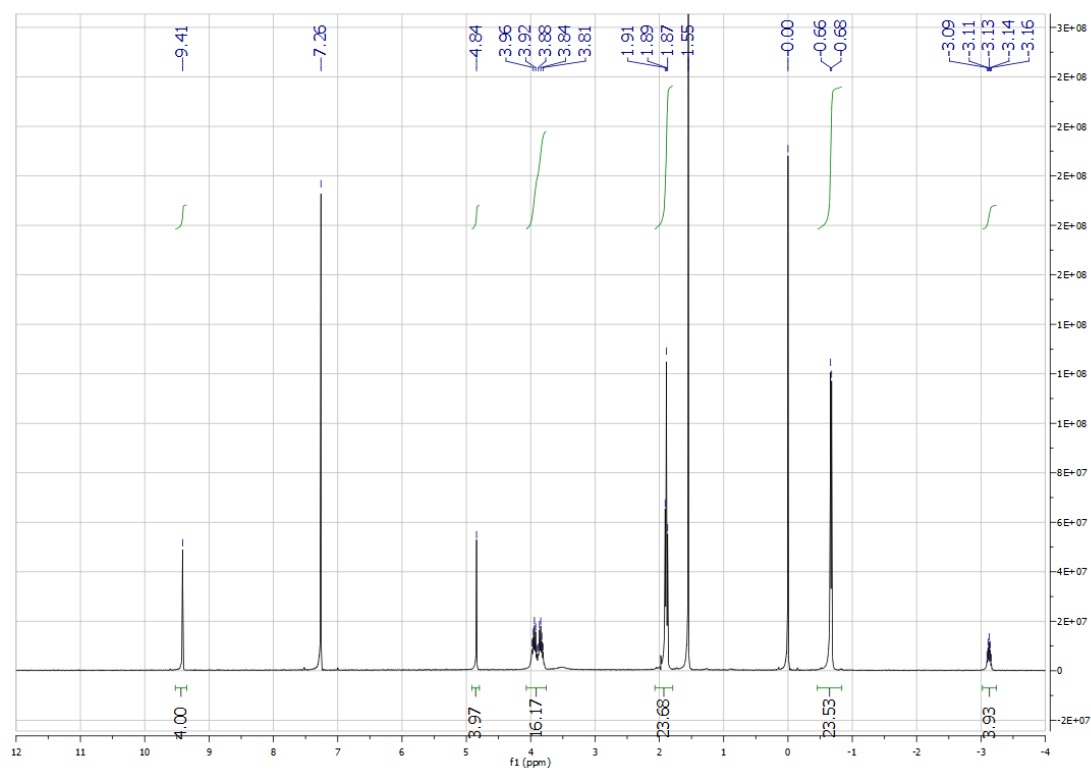


Fig. S9 ^1H NMR (400MHz, CDCl_3) spectrum of **2e**.

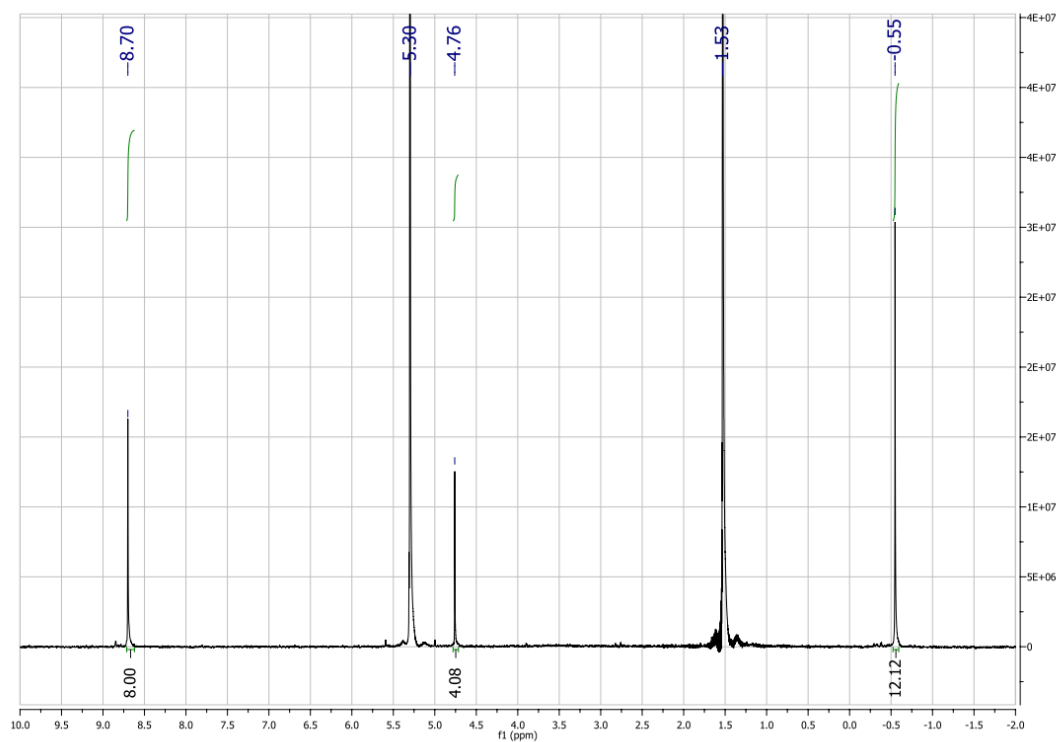


Fig. S10 ^1H NMR (400 MHz, CD_2Cl_2) spectrum of **2f**.

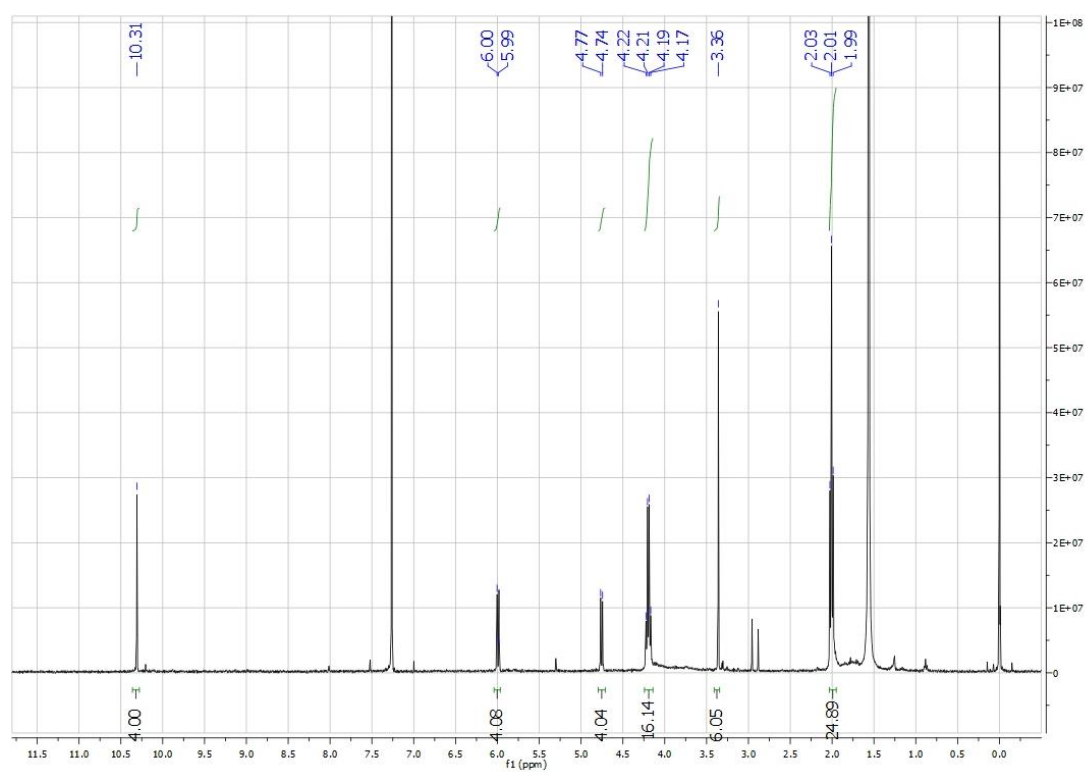


Fig. S11 ^1H NMR (400 MHz, CDCl_3) spectrum of **3**.

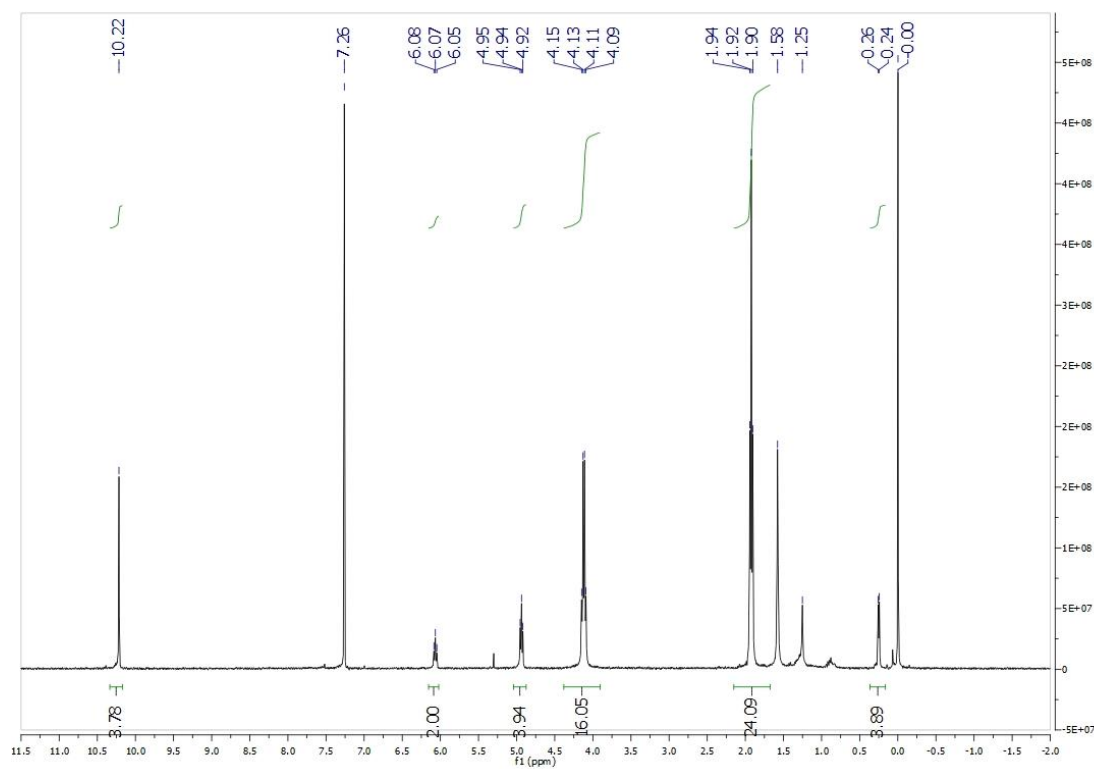


Fig. S12 ^1H NMR (400 MHz, CDCl_3) spectrum of **4**.

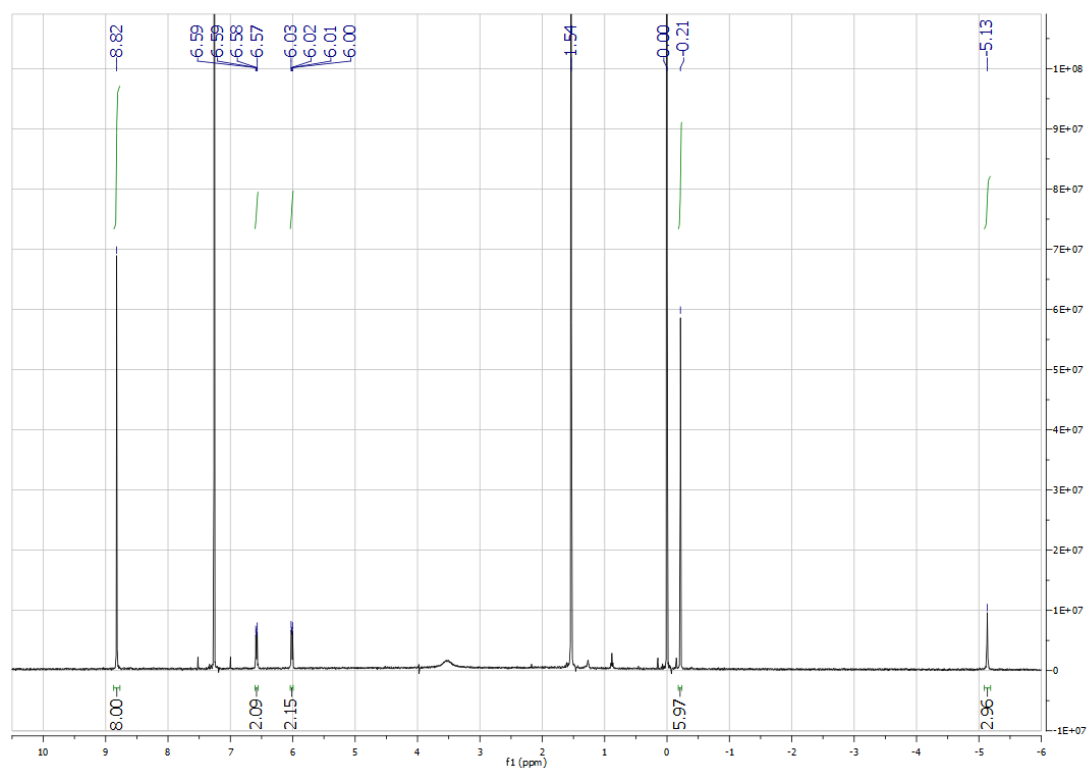


Fig. S13 ^1H NMR (400 MHz, CDCl_3) spectrum of **1d'**.

Table S1. Crystallographic data of **2a**, **2d**, **2e** and **2f**.

	2a·PF₆	2d·PF₆	2e	2f
Empirical formula	C ₅₈ H ₅₂ IrN ₈ ·F ₆ P·0.13(C H ₂ Cl ₂)	C ₅₄ H ₆₄ IrN ₈ ·F ₆ P	C ₅₄ H ₇₆ IrN ₈ ·F ₆ P·CH ₂ Cl ₂	C ₅₄ H ₂₄ F ₂₀ IrN ₈ ·0.25CF ₃ O ₃ S
Formula weight	1208.86	1162.32	1259.32	1394.28
λ [Å]	1.54178	1.54178	1.54184	1.54178
Crystal system	Triclinic	Monoclinic	Monoclinic	Monoclinic
Space group	P -1	C2/c	P2 ₁ /c	P2 ₁ /c
a [Å]	12.7322(6)	17.9784(6)	15.8369(12)	24.7628(7)
b [Å]	16.8417(10)	15.1240(6)	16.9326(12)	23.6873(7)
c [Å]	26.2843(12)	19.0318(6)	21.2999(16)	39.6486(13)
α [°]	77.893(3)	90	90	90
β [°]	84.194(2)	108.004(2)	97.044(3)	95.9405(17)
γ [°]	78.728(3)	90	90	90
V [Å ³]	5393.9(5)	4921.5(3)	5668.7(7)	23131.5(12)
Z	4	4	4	16
F(000)	2429	2360	2576	10868
ρ_{caled}	1.489	1.569	1.476	1.601
μ [mm ⁻¹]	5.745	6.140	6.220	5.567
Index	$h = -11 \rightarrow 11$ $k = -9 \rightarrow 15$ $l = -23 \rightarrow 23$	$h = -21 \rightarrow 16$ $k = -17 \rightarrow 16$ $l = -22 \rightarrow 22$	$h = -18 \rightarrow 18$ $k = -19 \rightarrow 10$ $l = -25 \rightarrow 24$	$h = -24 \rightarrow 24$ $k = -23 \rightarrow 23$ $l = -39 \rightarrow 39$
reflns	28233	52561	69982	206937
Independ	5880	4255	9578	24295
Parameter	1226	340	728	2885
final R	0.056	0.0287	0.045	0.107
(I>2s(I))	0.153	0.0701	0.126	0.286
GoF	1.08	1.11	1.07	1.06
largest	1.74/0.97	0.82/-0.67	1.64/-1.72	1.73/-1.19

$$^a R_1 = \Sigma ||F_o| - |F_c|| / \Sigma |F_o|, \quad ^b wR_2 = [\Sigma w(|F_o| - |F_c|)^2 / \Sigma w|F_o|^2]^{1/2}.$$

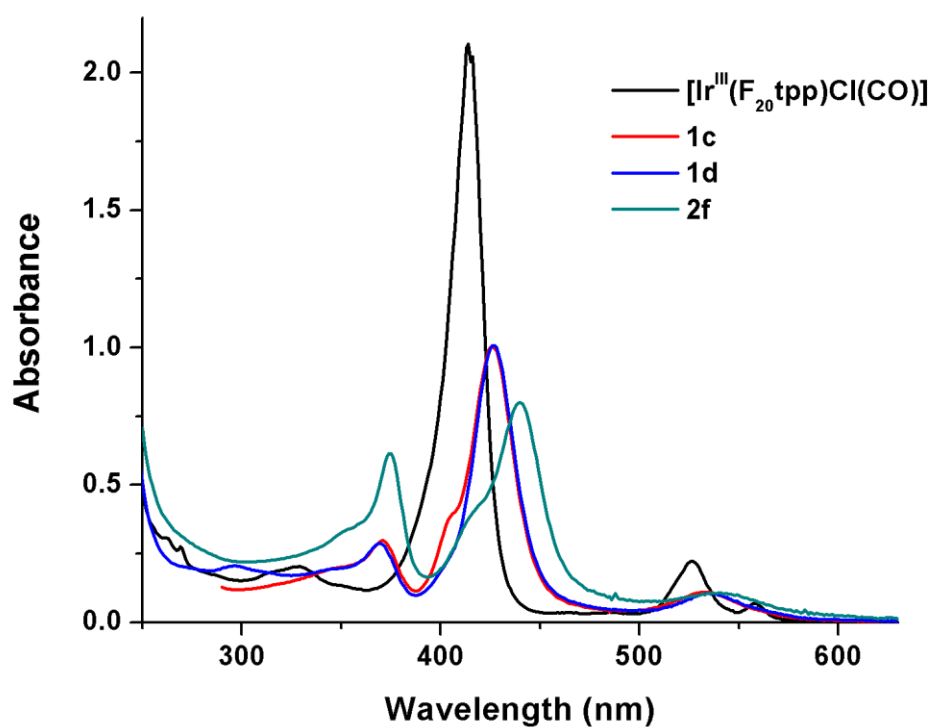


Fig. S14 UV-vis absorption spectra of $[\text{Ir}^{\text{III}}(\text{F}_{20}\text{tpp})\text{Cl}(\text{CO})]$, **1c** and **1d** in CHCl_3 and **2f** in CH_2Cl_2 at 8×10^{-6} M.

Table S2. UV-visible absorption data of **2e** in various organic solvents.

Solvent	$\lambda_{\text{max}}/\text{nm}$ (log ϵ)
CHCl_3	353 (sh) (4.49), 375 (4.82), 433 (4.82), 537 (4.09), 560 (4.02)
EtOAc	375 (4.79), 433 (4.78), 538 (4.01), 560 (3.94)
acetone	375 (4.78), 432 (4.78), 539 (4.01), 558 (3.93)
THF	375 (4.82), 432 (4.82), 536 (4.09), 556 (4.02)
toluene	375 (4.83), 433 (4.82), 537 (4.02), 560 (4.00)
MeOH	374 (4.75), 432 (4.74), 536 (4.08), 556 (3.90)
DMF	376 (4.78), 433 (4.79), 536 (4.00), 557 (3.93)

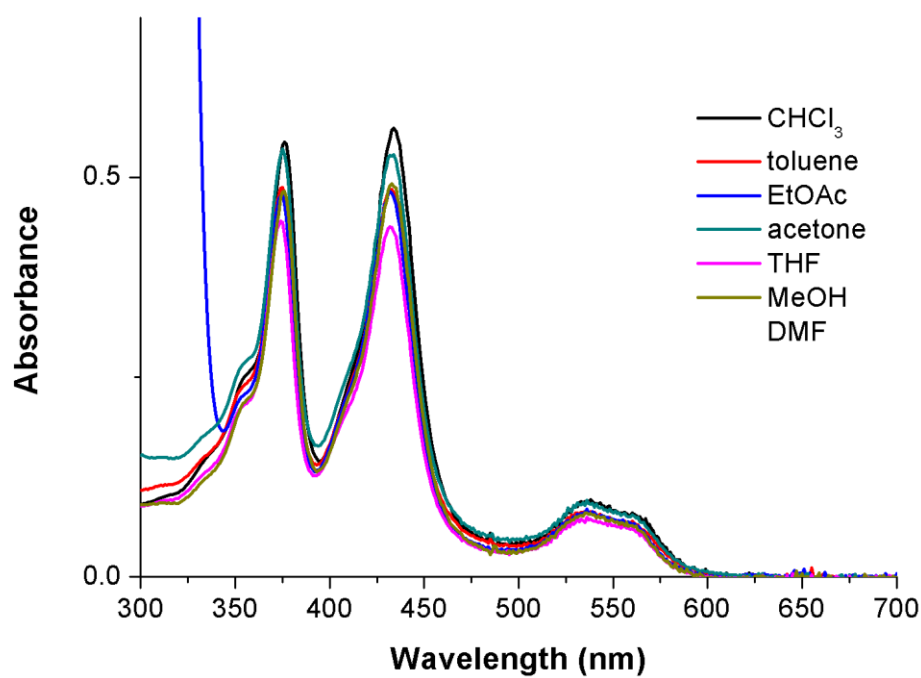


Fig. S15 UV-vis absorption spectra of **2e** in various organic solvents at 8×10^{-6} M.

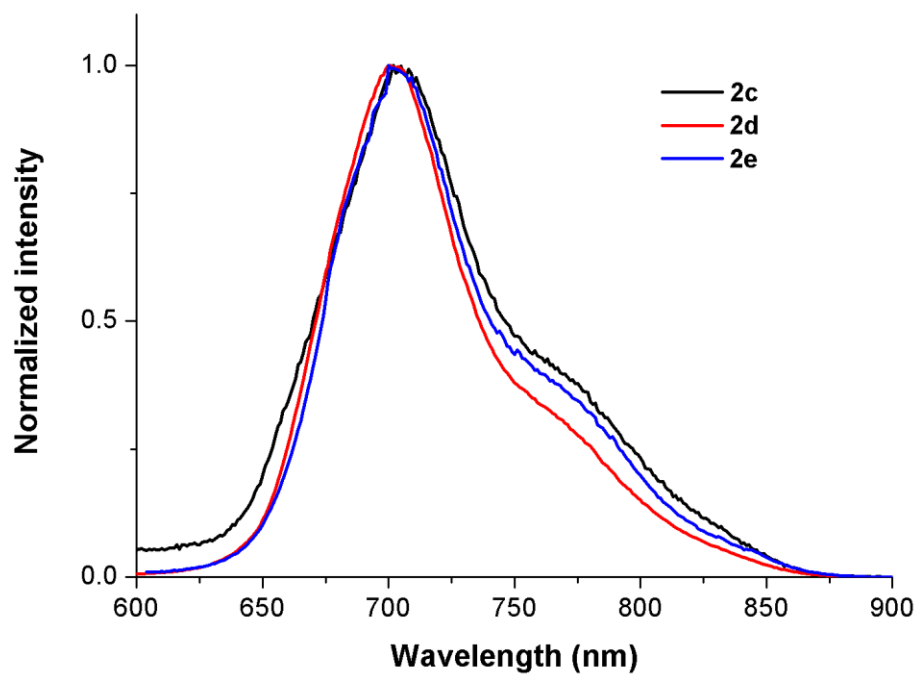


Fig. S16 Emission spectra of **2c–2e** in CHCl_3 .

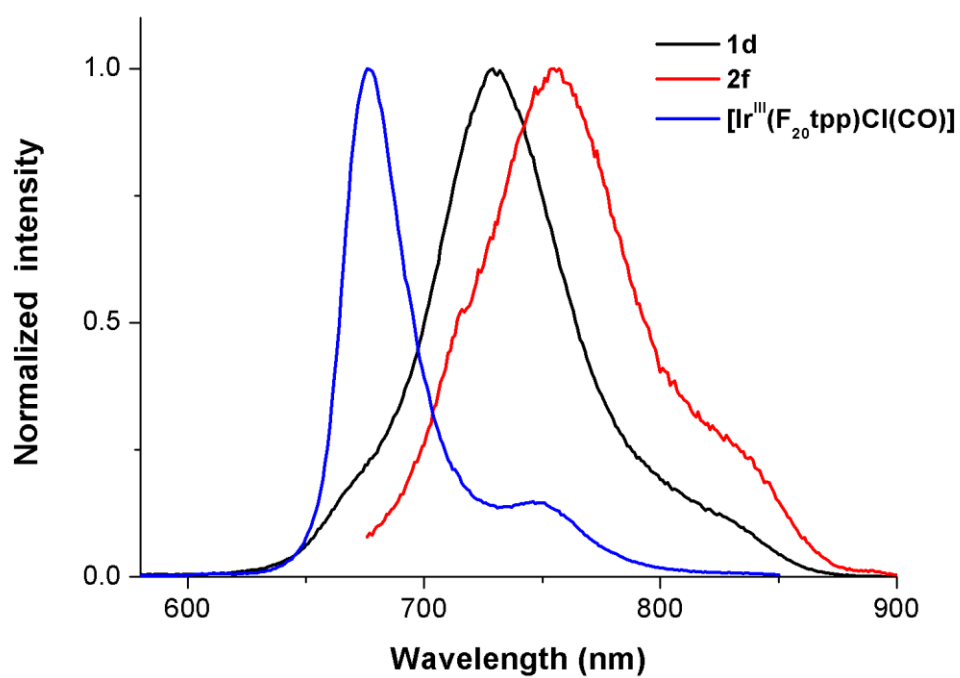


Fig. S17 Emission spectra of **1d**, **2f** and $[\text{Ir}^{\text{III}}(\text{F}_{20}\text{tpp})\text{Cl}(\text{CO})]$ in CHCl_3 .

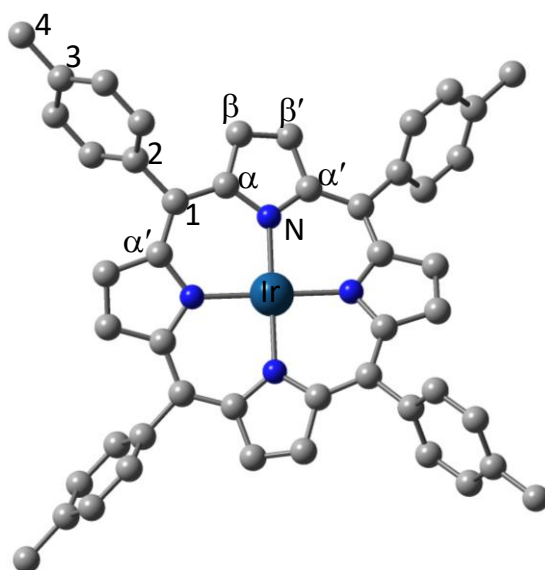


Fig. S18 DFT optimized structure of **2a**. (Hydrogen atoms and axial NHC ligands are omitted for clarity.)

Table S3. Natural transition orbitals (NTOs) of the hole (left) and electron (right) pair for S7/S8 and S9/S10 of **2a**.

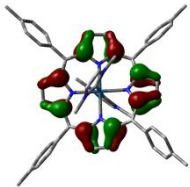
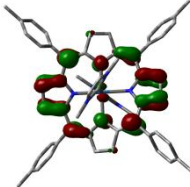
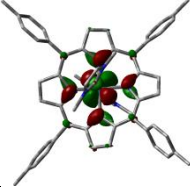
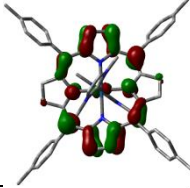
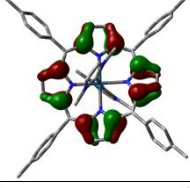
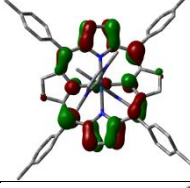
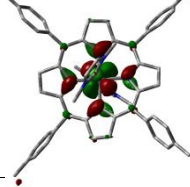
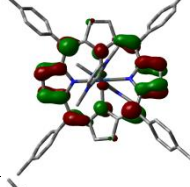
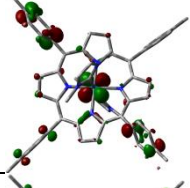
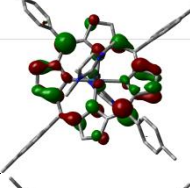
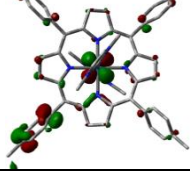
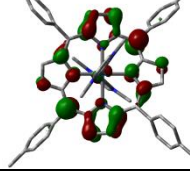
Excitation #	Hole	Electron	Type
S7 (68%)			$^1\pi-\pi^*$
S7 (32%)			$^1\text{MLCT}$
S8 (68%)			$^1\pi-\pi^*$
S8 (32%)			$^1\text{MLCT}$
S9(92%)			$^1\text{MLCT}/^1\text{ILCT}$
S10 (92%)			$^1\text{MLCT}/^1\text{ILCT}$

Table S4. The main experimental and calculated Raman bands and their corresponding vibrational mode assignments

Expt (cm ⁻¹)	DFT Calc (cm ⁻¹)	Assignments
1172 (enhancement @ 368.9 nm)	1157	Bending of the C α -C1-C α ' bond, including rocking of the Hs from pyrrole rings, very weak rocking of the Hs from tolyl rings.
1206 (enhancement @ 435.7 nm)	1192	Strong stretching of C3-C4, including rocking of the Hs from tolyl ring without any vibrational contribution from pyrrole rings.
1240 (enhancement @ 435.7 nm)	1231	Stretching of C1-C2 and rocking of the Hs on the tolyl ring (major), accompanied by bending deformation and rocking of the Hs within pyrrole rings (minor).
1281 (enhancement @ 368.9 nm)	1286	Symmetric and asymmetric stretching of the C α -C1-C α ' and weak stretching of the C1-C2 bond, including rocking of the Hs within pyrrole rings (major) and tolyl rings (minor).
1356	1344	Stretching of the C α -C1-C α ' bond and the C1-C2/C3-C4 bond, including rocking of the Hs within both tolyl rings and pyrrole rings.
1437 (enhancement @ 368.9 nm)	1448	Symmetric stretching of the C α -C1-C α ' bond and bending deformation of pyrroline rings, including rocking of the Hs within pyrrole rings (major) and on tolyl rings (minor).
1473	1489	C1-C2 and C3-C4 stretching, C β -C β ' stretching, including rocking of the Hs within both pyrrole rings and tolyl rings.
1521 (enhancement @ 368.9 nm)	1524	C β -C β ' stretching and bending of C α -N-C α ', including rocking of Hs within pyrrole rings (major) and on tolyl rings (minor), and weak C1-C2 stretching.
1607 (enhancement @ 435.7 nm)	1606	C-C bond stretching within tolyl rings and rocking of their Hs without any vibrational contribution from pyrrole rings.

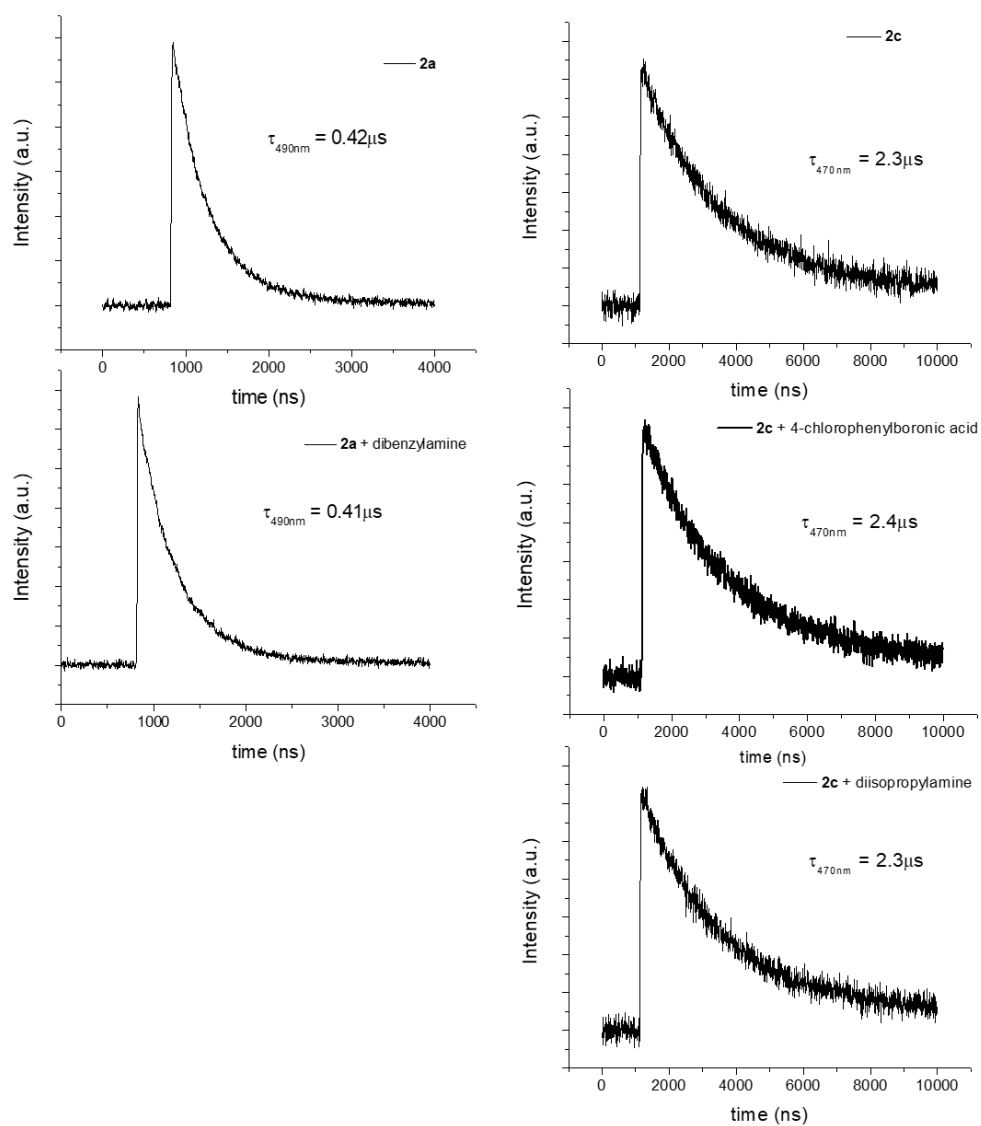
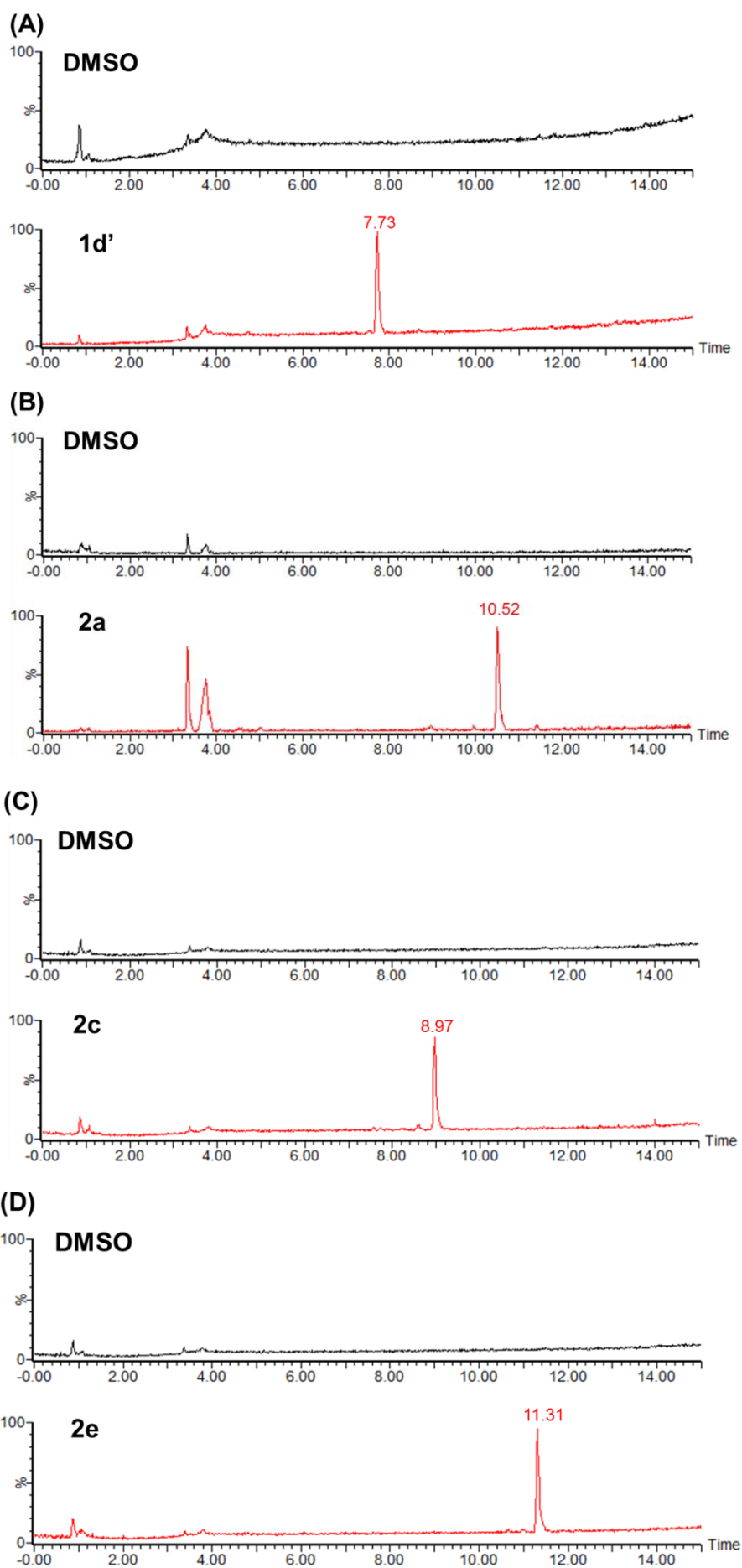


Fig. S19 $\Delta A_{490\text{nm}}$ decay curves of degassed MeCN solution of **2a** (10 μM) and **2a** (10 μM) with dibenzylamine (10 mM) as well as $\Delta A_{470\text{nm}}$ decay curves of degassed DMF solution of **2c** (10 μM), **2c** (10 μM) with 4-chlorophenylboronic acid (2 mM) and **2c** (10 μM) with diisopropylamine (8 mM).



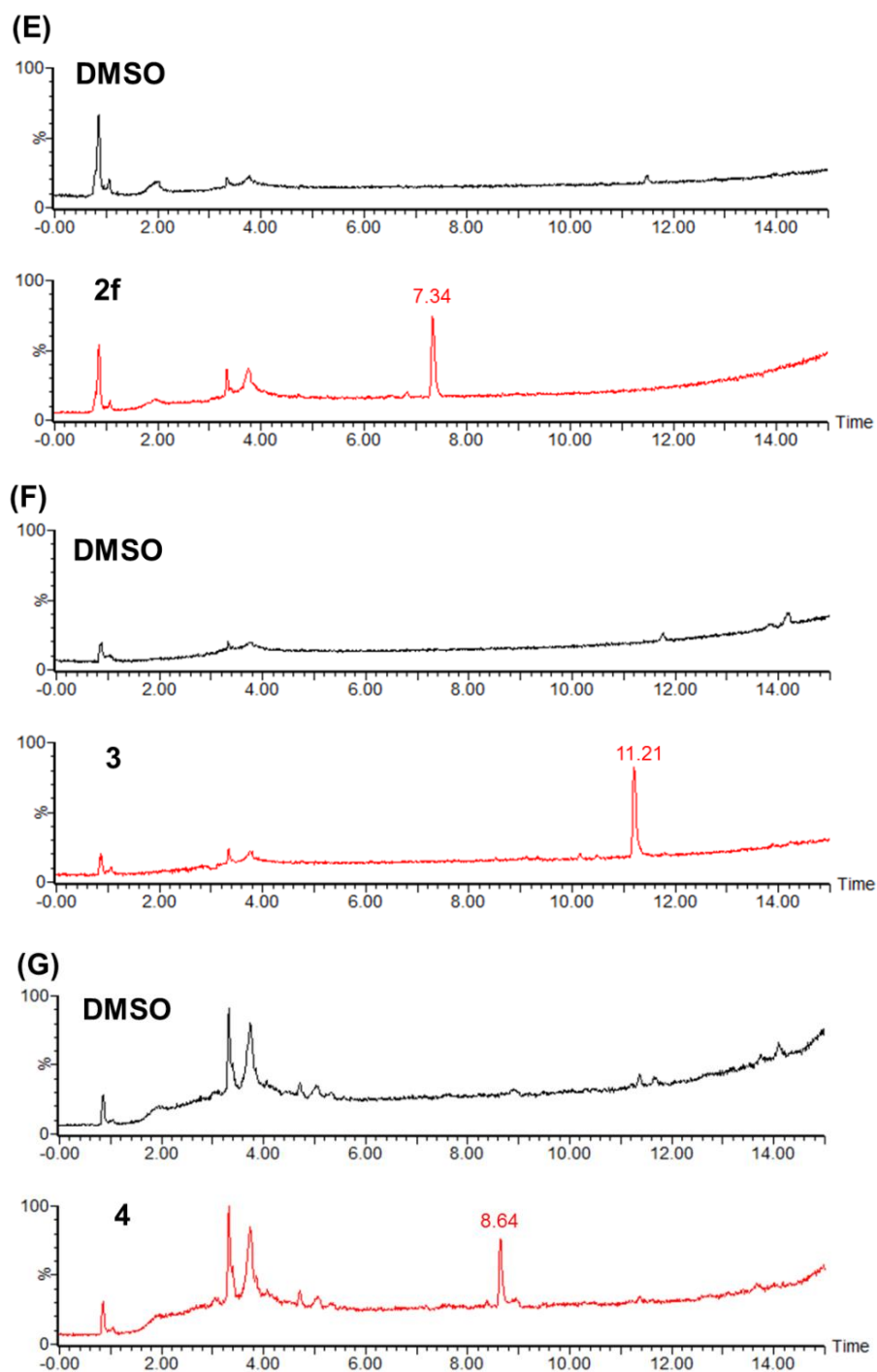
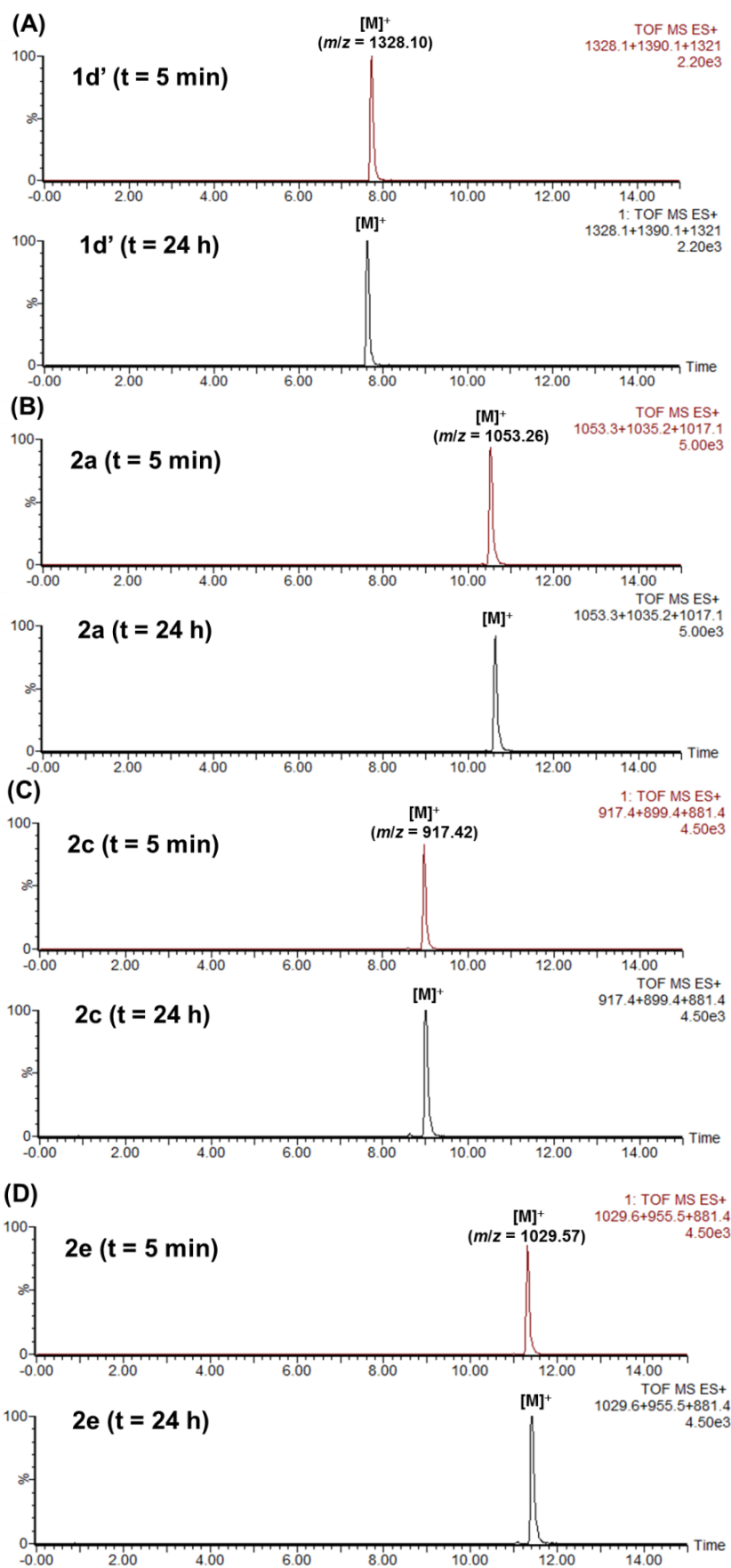


Fig. S20 UPLC-QTOF-MS chromatograms of complexes (A) **1d'**, (B) **2a**, (C) **2c**, (D) **2e**, (E) **2f**, (F) **3** and (G) **4** (1 μ M) in DMSO.



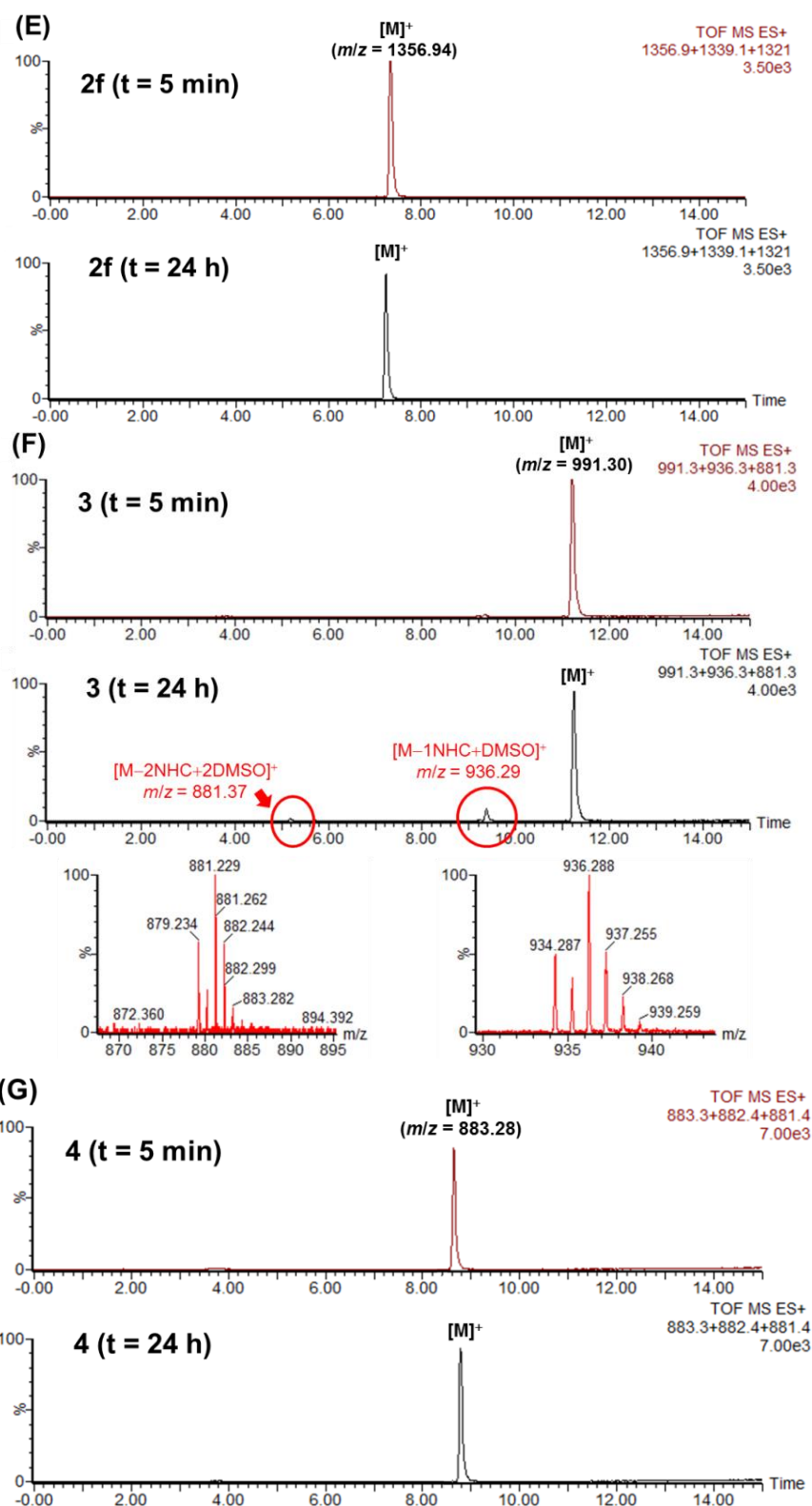


Fig. S21 Extracted-ion chromatograms of different complexes and possible DMSO-substituted forms after 5 min and 24 h incubation in DMSO.

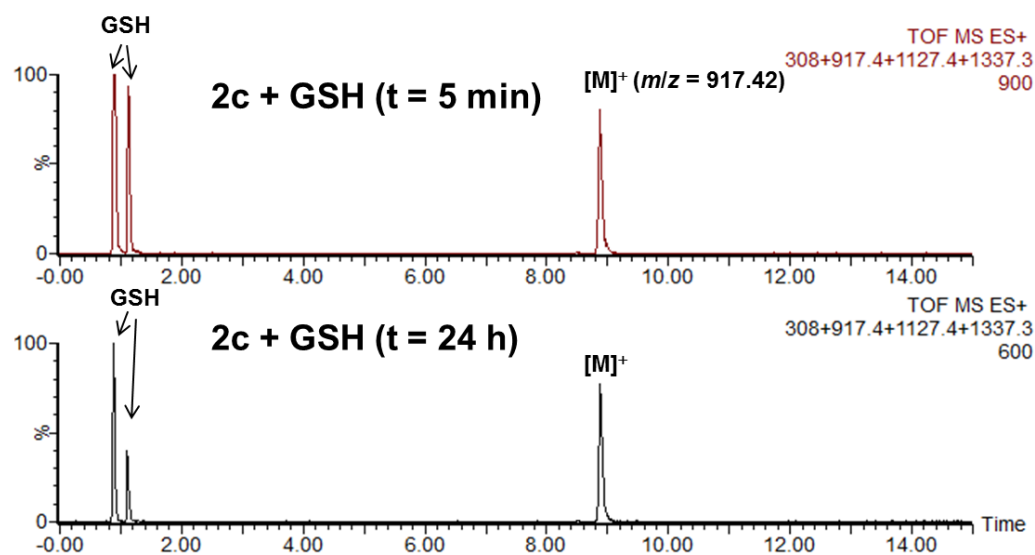


Fig. S22 Extracted-ion chromatograms of complex **2c** and possible glutathione-substituted forms after 5 min and 24 h incubation in DMSO/ammonium bicarbonate buffer (10 mM) (1:19, v/v).

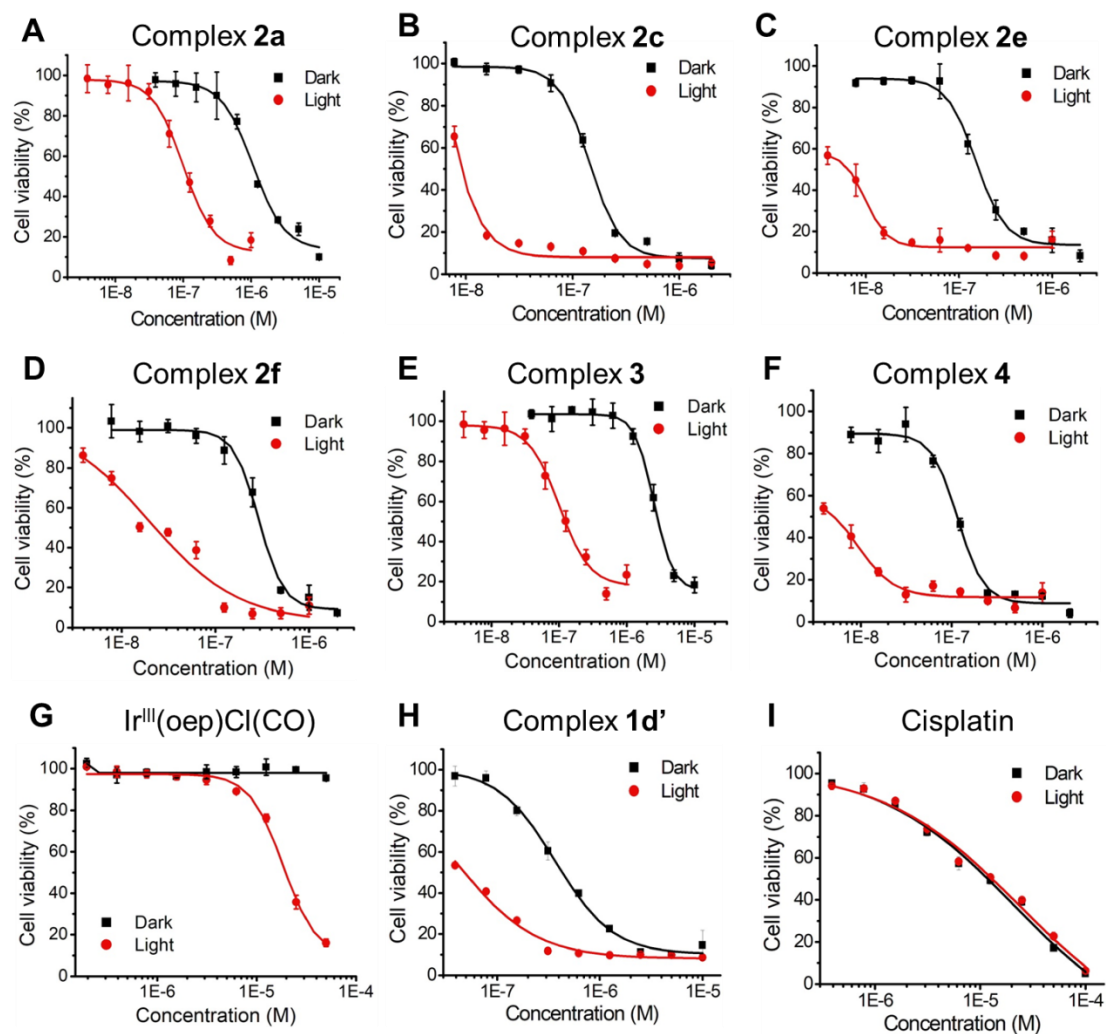


Fig. S23 Plots of cell viability of NCI-H460 lung cancer cells upon 72 h treatment with the iridium(III) porphyrin complexes and *cis*-platin in dark or under light irradiation (2.8 mW cm^{-2} for 1 h).

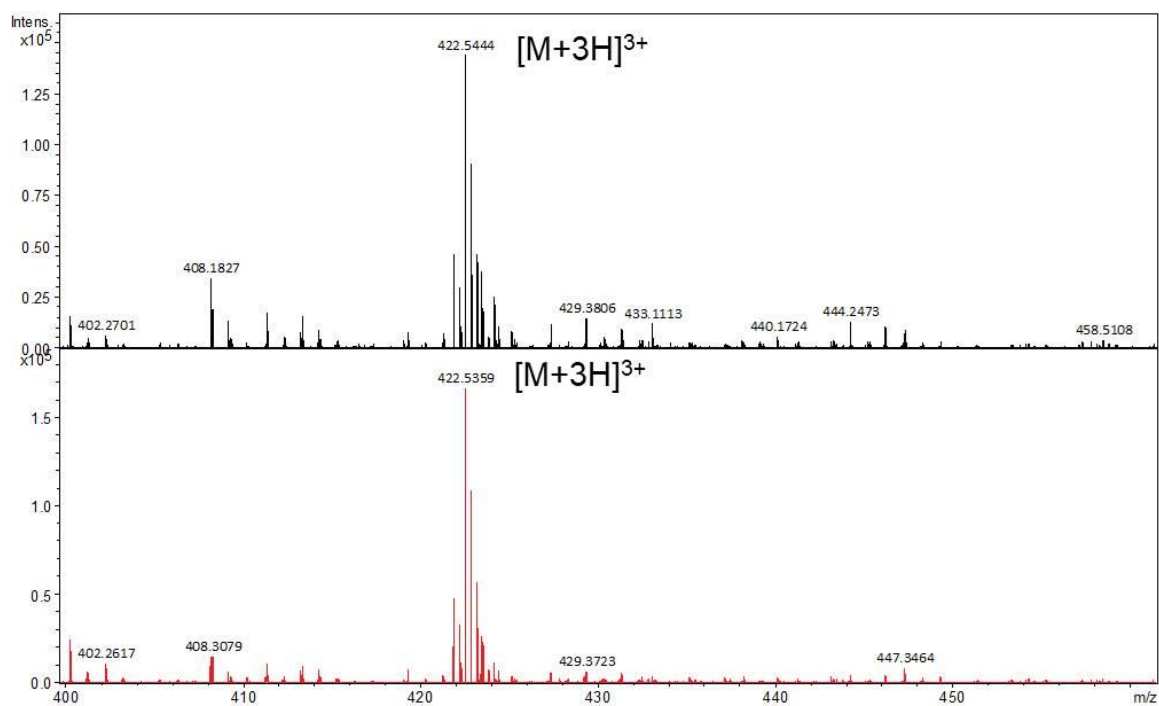


Fig. S24 ESI-MS spectra of triply charged peptide (RIMKCPGCWTA, 20 μM) at m/z 422.54 after incubation in dark (upper) or upon light irradiation (lower) for 1 h.

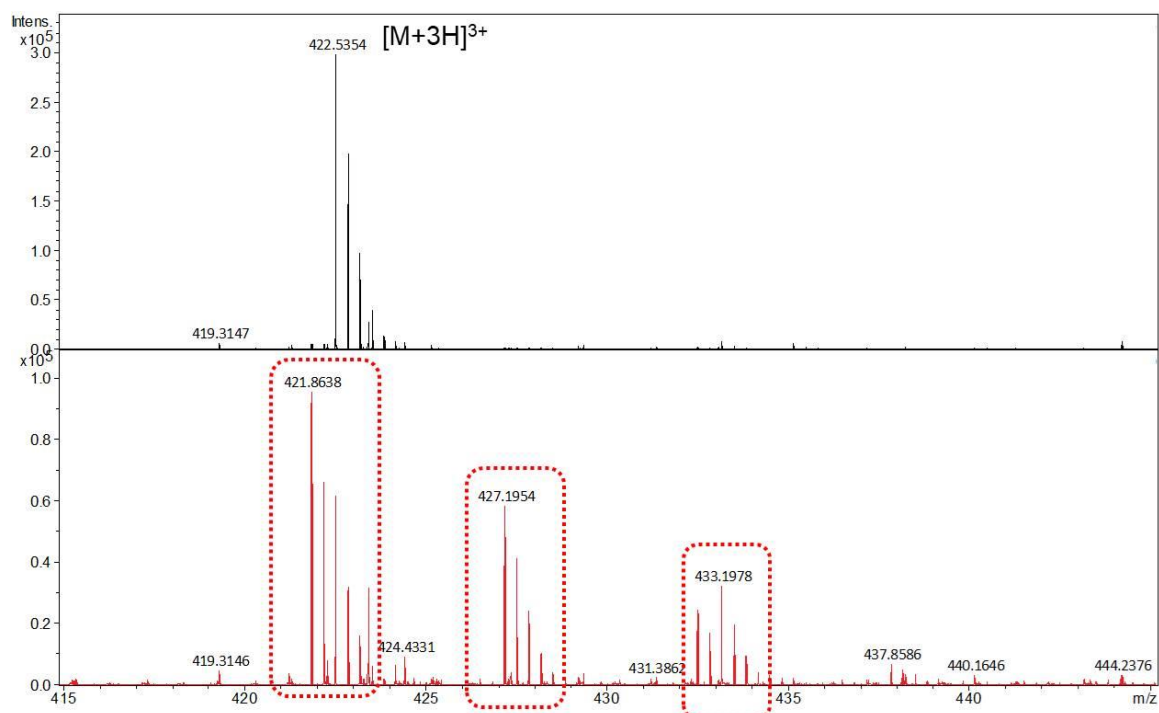


Fig. S25 ESI-MS spectra of triply charged peptide (RIMKCPGCWTA, 20 μ M) with complex **2c** (10 μ M) after incubation in dark (upper) or upon light irradiation (lower) for 1 h. The red dotted lines indicate the oxidative modification of the peptide.

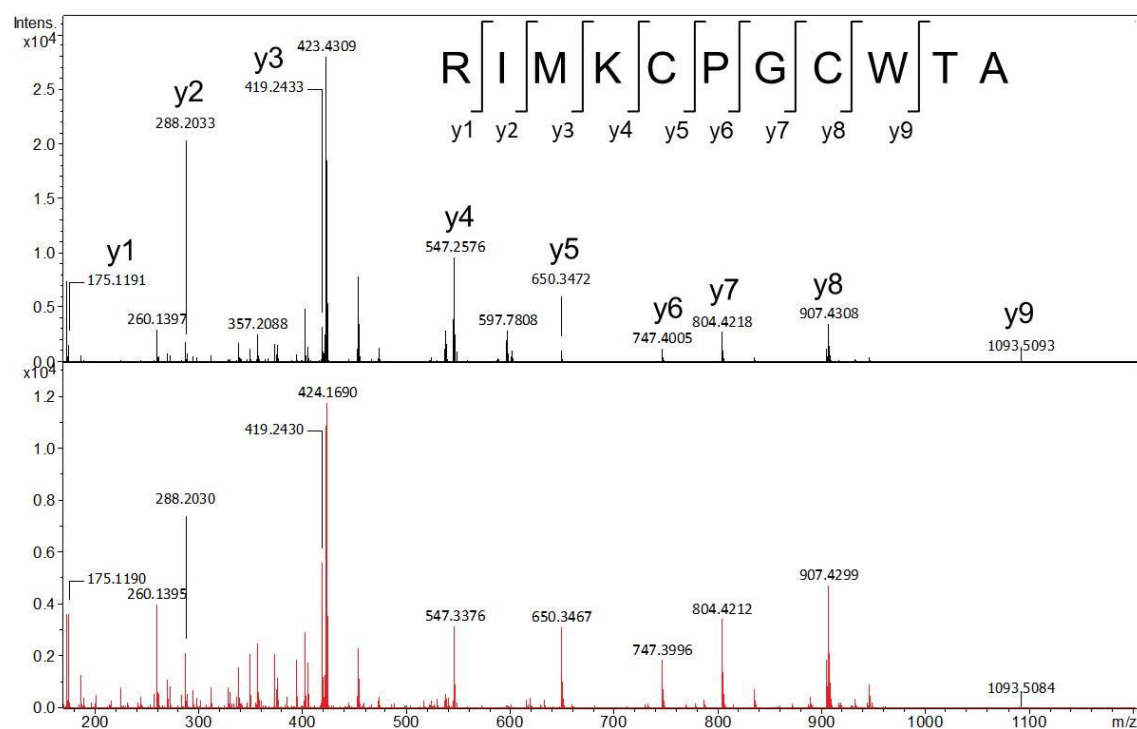
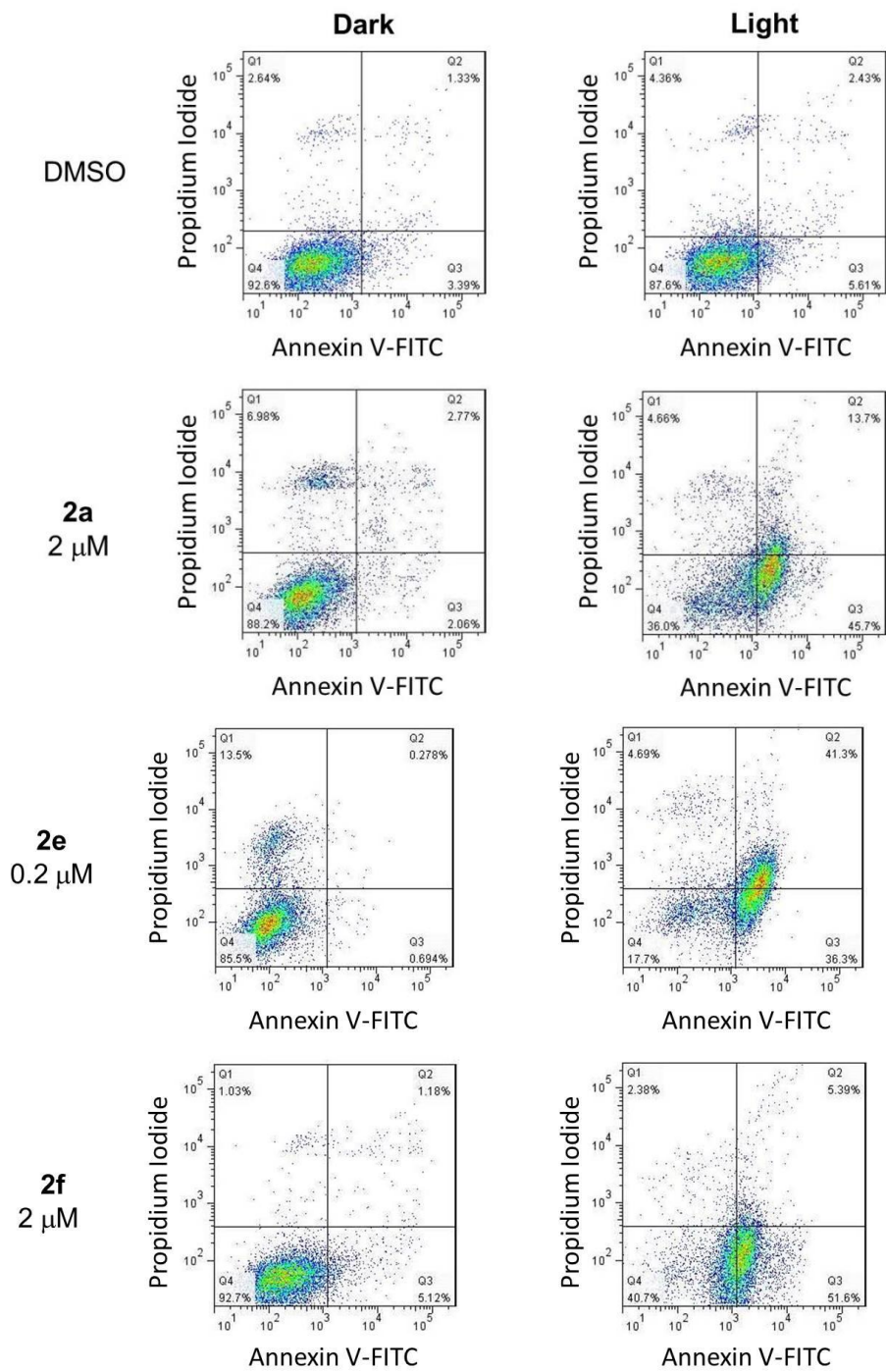
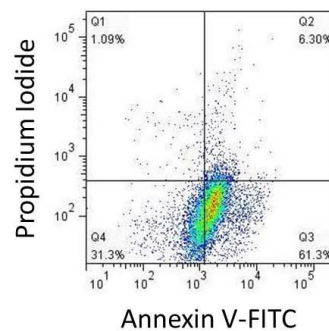
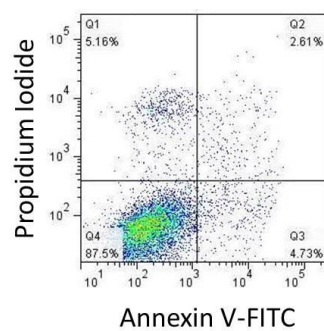


Fig. S26 MS/MS spectra of triply charged peptide (RIMKCPGCWTA, 20 μ M) at m/z 422.54 after incubation in dark (upper) or upon light irradiation (lower) for 1 h.



3
1 μ M



4
0.2 μ M

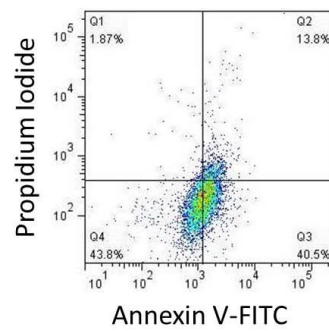
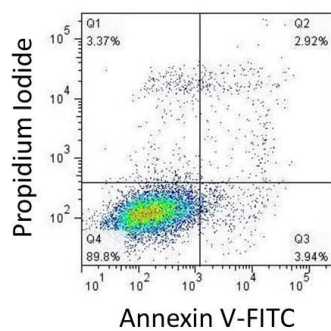


Fig. S27 Flow cytometric analysis of Annexin V/PI double stained NCI-H460 cells treatment with vehicle control, complex **2a**, **2e**, **2f**, **3** and **4** (14 h) in the absence or presence of light irradiation (2.8 mW cm^{-2} , 1 h).

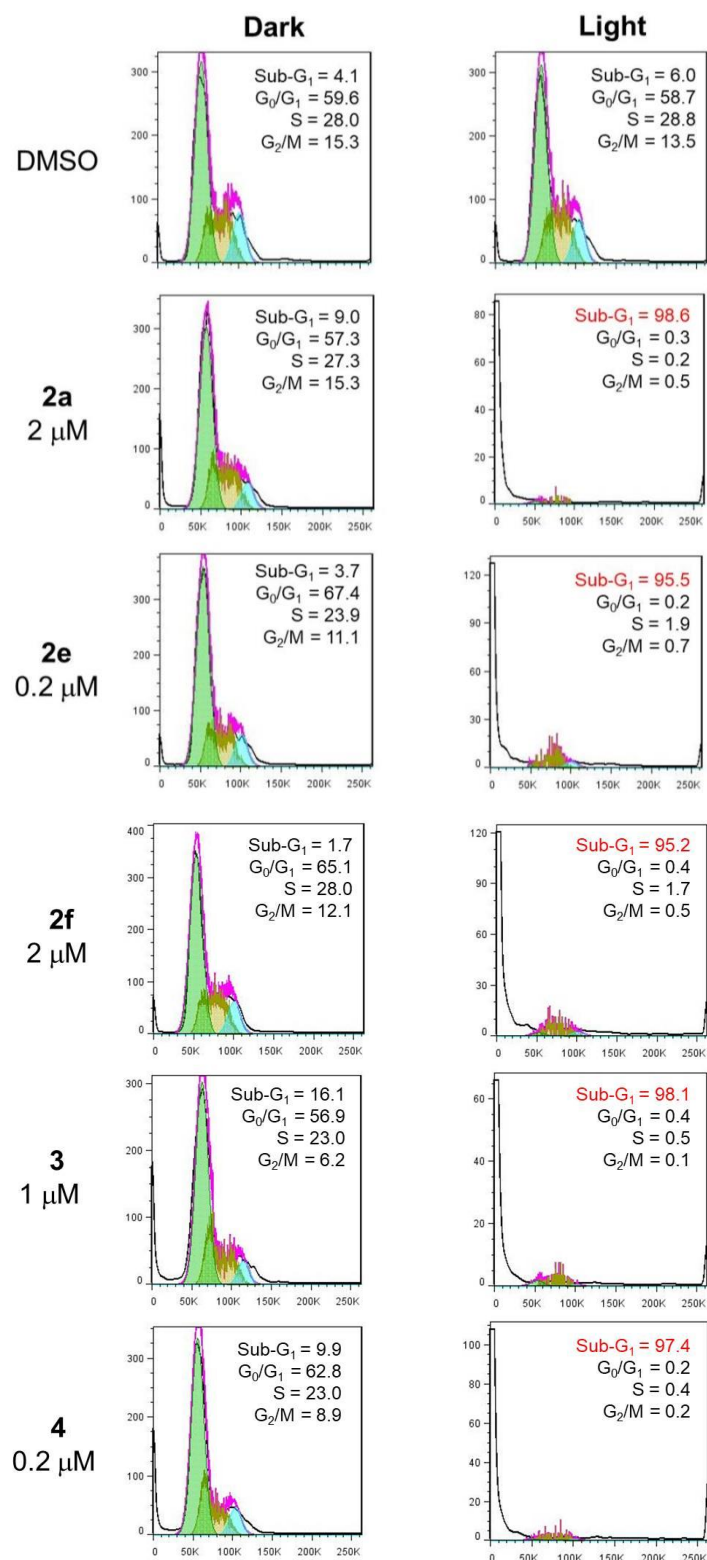


Fig. S28 Cell cycle progression analysis of DAPI-stained NCI-H460 cells treatment with vehicle control, complex **2a**, **2e**, **2f**, **3** and **4** (14 h) in the absence or presence of light irradiation (2.8 mW cm^{-2} , 1 h) by flow cytometry.

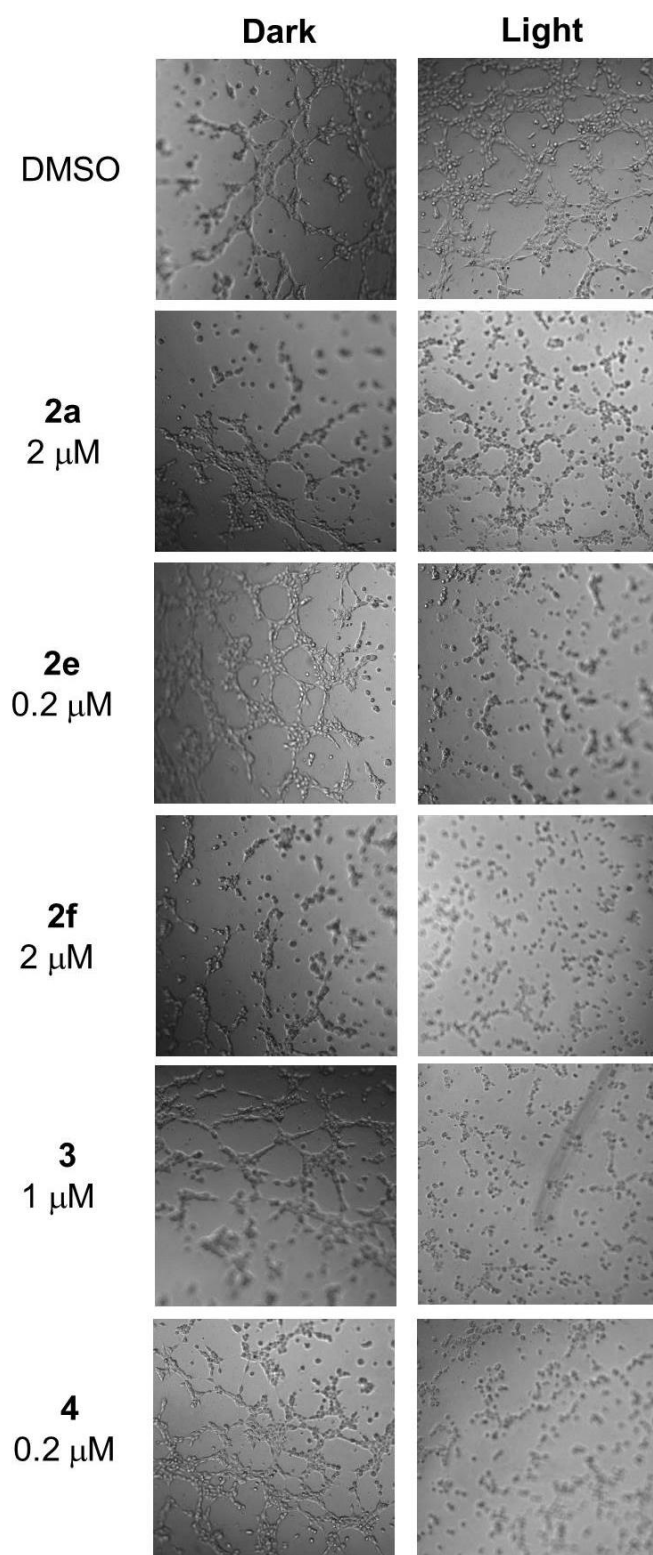


Fig. S29 Microscopic examination of the cellular tube formation of MS-1 endothelial cells after treatment with vehicle control, complex **2a**, **2e**, **2f**, **3** and **4** (1 h) in the absence or presence of light irradiation (2.8 mW cm^{-2} , 1 h).

Table S5. Mass errors of the fragments detected from Trx peptide (RIMKCPGCWTA) at m/z 422.54 by ESI-MS/MS.

Assignment	Observed (m/z)	Theoretical (m/z)	Mass error (ppm)
[y1] ⁺	175.1190	175.1195	-2.86
[y2] ⁺	288.2030	288.2036	-2.08
[y3] ⁺	419.2430	419.2441	-2.62
[y4] ⁺	547.3376	547.3390	-2.56
[y5] ⁺	650.3467	650.3482	-2.31
[y6] ⁺	747.3996	747.4010	-1.87
[y7] ⁺	804.4212	804.4224	-1.49
[y8] ⁺	907.4299	907.4316	-1.87
[y9] ⁺	1093.5084	1093.5109	-2.29

Table S6. Mass errors of the fragments detected from modified Trx peptide (RIMK**C**PG**C**WTA) at m/z 421.86 by ESI-MS/MS. Blue label represents the site for disulfide bond formation.

Assignment	Observed (m/z)	Theoretical (m/z)	Mass error (ppm)
[y1] ⁺	175.1187	175.1195	-4.57
[y2] ⁺	288.2025	288.2036	-3.82
[y3] ⁺	419.2423	419.2441	-4.29
[y4] ⁺	547.3367	547.3390	-4.20
[y5]⁺	650.3456	650.3476	-3.08
[y6] ⁺	747.3982	747.4004	-2.94
[y7] ⁺	804.4197	804.4218	-2.61
[y8]⁺	905.4135	905.4154	-2.10
[y9] ⁺	1091.4931	1091.4947	-1.47

Table S7. Mass errors of the fragments detected from modified Trx peptide (RIMKCPGCWTA) at m/z 427.20 by ESI-MS/MS. Red label indicates the oxidative site and blue label represents the site for disulfide bond formation.

Assignment	Observed (m/z)	Theoretical (m/z)	Mass error (ppm)
[y1] ⁺	175.1185	175.1195	-5.71
[y2] ⁺	288.2024	288.2036	-4.16
[y3+O] ⁺	435.2369	435.2384	-3.45
[y4] ⁺	563.3312	563.3333	-3.73
[y5] ⁺	666.3409	666.3426	-2.55
[y6] ⁺	763.3931	763.3953	-2.88
[y7] ⁺	820.4142	820.4167	-3.05
[y8] ⁺	921.4080	921.4103	-2.50
[y9] ⁺	1107.4881	1107.4896	-1.35

Table S8. Mass errors of the fragments detected from modified Trx peptide (RIMKCPG**C**WTA) at m/z 433.20 by ESI-MS/MS. Red label indicates the oxidative site.

Assignment	Observed (m/z)	Theoretical (m/z)	Mass error (ppm)
[y1] ⁺	175.1186	175.1195	-5.14
[y2] ⁺	288.2025	288.2036	-3.81
[y3+O]⁺	435.2375	435.2384	-2.07
[y4] ⁺	563.3312	563.3333	-4.05
[y5] ⁺	666.3399	666.3426	-4.05
[y6] ⁺	763.3926	763.3953	-3.54
[y7] ⁺	820.4139	820.4168	-3.53
[y8+O]⁺	939.4150	939.4209	-6.28
[y9] ⁺	1125.4984	1125.5002	-1.60